University of Alberta

Laboratory Studies of Suspended Frazil Ice Particles

by

Vincent John McFarlane

A thesis submitted to the Faculty of Graduate Studies and Research
in partial fulfillment of the requirements for the degree of

Master of Science
in
Water Resources Engineering

Department of Civil and Environmental Engineering

Spring 2014
Edmonton, Alberta

Abstract

The physical and kinematic properties of frazil ice particles have proven difficult to measure with any accuracy in the past. As a result, little is known about the size distribution, thickness, aspect ratio, and rise velocity of these particles, making it impossible to develop accurate mathematical models of the formation, development, and transport of frazil ice. To address this lack of data, a digital image acquisition system was developed capable of capturing high-resolution, cross-polarised photographs of suspended frazil ice particles in a laboratory environment. An algorithm was written to process these images and calculate the diameter of individual particles. A lognormal distribution was found to offer a good fit to the particle diameters. This image acquisition and processing system was also applied to rising frazil ice particles and the effects of particle thickness, diameter, aspect ratio, and orientation on the rise velocity of frazil ice in quiescent water was studied.

Acknowledgments

The author would like to thank his supervisors, Dr. Faye Hicks and Dr. Mark Loewen, for their assistance and guidance in all aspects of this project. All of the time and effort they have put into helping him is very much appreciated. Thank you as well to Dr. Paul Myers for being on the oral examining committee and Dr. Evan Davies for chairing the exam.

Thank you to Perry Fedun and Chris Krath for their technical assistance, especially in designing and constructing the experimental apparatus in the lab, and to Christine Hereygers and Drs. David Sego and Derek Martin for facilitating access to the cold room facility.

This research was supported by the Natural Sciences and Engineering Research Council of Canada (NSERC), which is gratefully acknowledged.

The author would also like to thank his family and friends for their love and support throughout the Master's program, and his fellow water resources graduate students, specifically Dr. Tadros Ghobrial for introducing him to frazil ice and acting as an additional mentor throughout his studies.

Table of Contents

List of Tables

List of Figures

Chapter 1: Introduction

The formation of frazil ice particles occurs early in the river freeze-up process, when the turbulent river flow becomes supercooled (suspended frazil ice particles produced in the lab are shown in Figure 1-1). The concentration of these disc-shaped particles rises if supercooling persists, resulting in higher frazil ice concentrations and the formation of frazil flocs when particles collide and freeze to each other (Figure 1-2). When the flocs become large enough that their buoyancy can overcome the turbulence, they rise to the surface where they are exposed to the cold air and freeze into a crusty ice layer, forming frazil pans (Figure 1-3). These pans will in turn collide with each other and freeze into larger accumulations of frazil pans called rafts which, at high enough concentrations, may lead to bridging of the channel and the progression of an ice front in the upstream direction (Figure 1-4).

In addition to freezing to each other, frazil particles attach themselves to nearly any surface they come in contact with while in the 'active' state (i.e. while the water surrounding them remains supercooled). This has been known to cause problems for water intakes along the river, as the trash racks on an intake can quickly become obstructed by a large accumulation of frazil. As a result, the flow into the intake can be restricted or even halted entirely in extreme cases, forcing industrial plants to shut down until the blockage can be cleared (Richard and Morse 2008). Frazil ice particles can also freeze onto the bed material of a river forming anchor ice (Figure 1-5), which can reduce the flow area in a channel,

raise the bed level, alter the flow velocity, and seriously impact fish habitat (e.g. Brown et al. 2011; Stickler et al. 2010). However, if the rise velocity of the frazil particles is large enough to overcome the vertical component of the turbulent velocity fluctuations in the flow, frazil ice particles may remain at the water surface rather than becoming entrained in the flow, leading to the formation of a skim ice cover (Figure 1-6) (Matoušek 1992).

It is important to be able to predict frazil ice events in order to prepare for their consequences, which requires accurate models of the river freeze-up process. In order to model these events properly we must understand the physical properties of frazil ice, such as the size distribution and shape of the particles, as well as the kinematics of frazil transport, of which rise velocity is a very important aspect. Increased knowledge of these properties will aid in the development of models able to determine when and where frazil ice particles will form in the flow, in what concentration, and where this frazil ice will ultimately end up. Measurements of the size distributions and concentrations of frazil ice events occurring in the field would greatly assist in this type of model development, but there is currently no proven method for accurately measuring these properties in situ. Recently, several studies have demonstrated that upward looking sonars can detect frazil particles suspended in the flow (Ghobrial et al. 2013a; b; Marko and Jasek 2010a; b). However, estimates of frazil concentrations and sizes made using upward looking sonars need to be validated with direct observations (e.g.

photographic measurements) to demonstrate that this technique provides accurate results.

Although turbulence exists in real river flows, it is important to understand the rise velocity of frazil ice particles in quiescent water in order to enhance our knowledge of frazil transport, analogous to the study of settling velocity in sediment transport. The rise velocity in quiescent water is also an important property in determining if individual frazil particles will overcome the turbulence and rise to the surface leading to the formation of skim ice; remain in suspension until flocs large enough to overcome the turbulence rise, forming frazil pans; or adhere to the river bed and form accumulations of anchor ice. A number of theoretical expressions have been proposed for predicting the rise velocity of frazil particles (Morse and Richard 2009) but there is a significant lack of experimental data to verify these equations.

The objective of this study was to increase our understanding of the physical properties and kinematics of frazil ice particles. This was achieved through a series of laboratory experiments in which high-resolution, cross-polarised digital images were captured of frazil ice particles produced in a specially designed frazil ice tank. Increased knowledge of the diameter, thickness, and rise velocity of frazil ice particles will help to improve our understanding of how an ice cover forms on rivers of various properties. This information in turn could aid in the development of future numerical models of the entire freeze-up process, from the

formation of the first frazil ice particles through to the formation of a solid ice cover.

1.1 Size Distribution, Particle Thickness, and Aspect Ratio

Daly and Colbeck (1986) studied the size distributions of frazil ice at 8 different locations along the length of a 36.6 m long flume located in a cold room. Using a 35 mm camera and microscope combination, very high resolution images were captured, enabling them to observe particles as small as 35 μm in diameter. However, the largest particles observed by Daly and Colbeck (1986) were only approximately 0.5 mm in diameter, whereas subsequent studies (e.g. Clark and Doering (2006)) have documented particles as large as 5 mm. This could potentially have been caused by the short amount of time that the particles had to grow while traveling down the length of the flume. In their experiments, water was supercooled using a heat exchanger prior to entering the head box of the flume where it was seeded with ice crystals to initiate frazil formation. These particles would continue to grow and develop for the remainder of their time in the flume, but upon exiting the flume the water was warmed up to about 0.01°C in the sump, and was then heated to about 0.03 to 0.05°C while passing through the pump and piping. Through this process, all existing frazil particles were melted before the water re-entered the flume. Based on the size distributions that they observed, Daly and Colbeck (1986) recommended a lognormal distribution to describe frazil ice particles. Average diameter to thickness ratios, or 'aspect ratios', were also presented by Daly and Colbeck (1986) for a few of the measurement locations along the flume, and were found to range from 6.37 to

9.61. They found that the mean ratio increased in the downstream direction of the flume, and hypothesised that this may be due to the crystal diameter increasing faster than the thickness.

Doering and Morris (2003) developed a system to capture cross-polarised digital images of frazil ice particles produced in a counter-rotating flume. The images had a resolution of 640 x 480 pixels and a 16.5 x 12.0 cm field of view, resulting in a pixel size of 0.25 mm/pixel. A digital image processing algorithm was developed by Doering and Morris (2003) that identified and calculated the diameter of each frazil particle. Clark and Doering (2006) continued this research using a higher resolution camera (1024 x 1300 pixels) and a 25 mm lens that acquired images with a pixel size of 55 μm/pixel. They assumed that an object in the image needed to have a diameter of at least three pixels before it was identified as a frazil particle, meaning the minimum particle size observable was 165 μm. Overall, 793 frazil particles were measured by Clark and Doering (2006) with a mean diameter of 1.31 mm and standard deviation of 0.86 mm. They also concluded that a lognormal distribution fit the data well, in agreement with Daly and Colbeck (1986). Particle thicknesses were also measured by Clark and Doering (2006) for approximately 160 particles with an average diameter of 3.35 mm, average thickness of 0.23 mm, and diameter to thickness or 'aspect' ratios ranging from 12.9 to 16.33.

1.2 Rise Velocity

Experimental studies of the rise velocity of frazil ice particles are scarce. In fact, we are only aware of two previous studies that have been carried out for the purpose of measuring the rise velocity of real frazil ice particles. Gosink and Osterkamp (1983) performed the first such study by measuring the rise velocity of frazil ice particles produced both in the lab and in the Chatanika River, Alaska. Particles were timed as they rose in a graduated cylinder using a stopwatch, and their diameters were estimated to the nearest 0.5 mm by comparing them to the graduations on the cylinder. Frazil ice particles ranging in diameter from 1 to 6 mm with rise velocities from 3 to 22 mm/s were observed, although it was noted that due to experimental difficulties these results must be considered preliminary. A force balance model for predicting the terminal rise velocity of a disc rising with its flat face aligned with the horizontal plane was also derived by Gosink and Osterkamp (1983), and they found that their data could be enveloped by curves corresponding to aspect ratios of 10 and 80. They ultimately concluded that an aspect ratio of 20 was a representative value for all frazil particles.

A similar study was performed by Wuebben (1984) in the laboratory. He also timed particles using a stopwatch while they rose in a graduated cylinder, and estimated particle diameters to the nearest 0.25 mm. Diameters ranging from 0.25 to 4 mm were observed and rise velocities ranged from 0.8 to 5.5 mm/s. By plotting a number of curves corresponding to aspect ratios from 10 to 200 and comparing them with a theoretical power law he derived for his data, Wuebben

(1984) determined the aspect ratios for his data set ranged from approximately 20 to 90. He then assumed that frazil particles grow preferentially with increasing diameter and that their thickness remains essentially constant, and thereby estimated that a constant disc thickness of 0.05 mm represented his data in the 1 to 4 mm diameter range quite well.

In addition to these studies a number of researchers have proposed theoretical relationships between particle diameter and rise velocity (Morse and Richard 2009), and these are described in detail in Chapter 3. However, due to the lack of experimental data, it was impossible for them to verify the accuracy of any of these equations.

1.3 Objectives

The goal of this study was to address the lack of measurements of the size distribution and rise velocity of frazil ice particles. First, a digital image acquisition and processing system similar to those described by Doering and Morris (2003) and Clark and Doering (2006, 2008), but employing a higher resolution camera, was developed and tested with the objective of capturing and measuring frazil ice particles over as wide a range of sizes as possible. This system was designed to capture high-resolution cross-polarised images of suspended frazil ice particles produced in a laboratory frazil ice tank, and to correctly identify and measure the properties of individual particles. A description of this system and experimental results are presented in Chapter 2.

Secondly, the image acquisition system was used to capture sequences of high-resolution images of frazil ice particles as they ascended between two cross-polarising filters. These images were used to compute accurate estimates of both the diameter and rise velocity of frazil particles, so as to address the need for reliable experimental data for comparison to theoretical relationships. An increased understanding of frazil rise behaviour in quiescent water is a first step in improving our knowledge of how these particles behave in turbulent flows. The thickness and aspect ratio of frazil ice particles were also measured in these experiments in order to test the hypothesis that frazil ice particles grow preferentially in the direction normal to the *c*-axis (i.e. with increasing diameter), and determine whether the assumption of a constant aspect ratio (Gosink and Osterkamp 1983) or a constant thickness (Wuebben 1984) is more valid. The details of this study component are presented in Chapter 3.

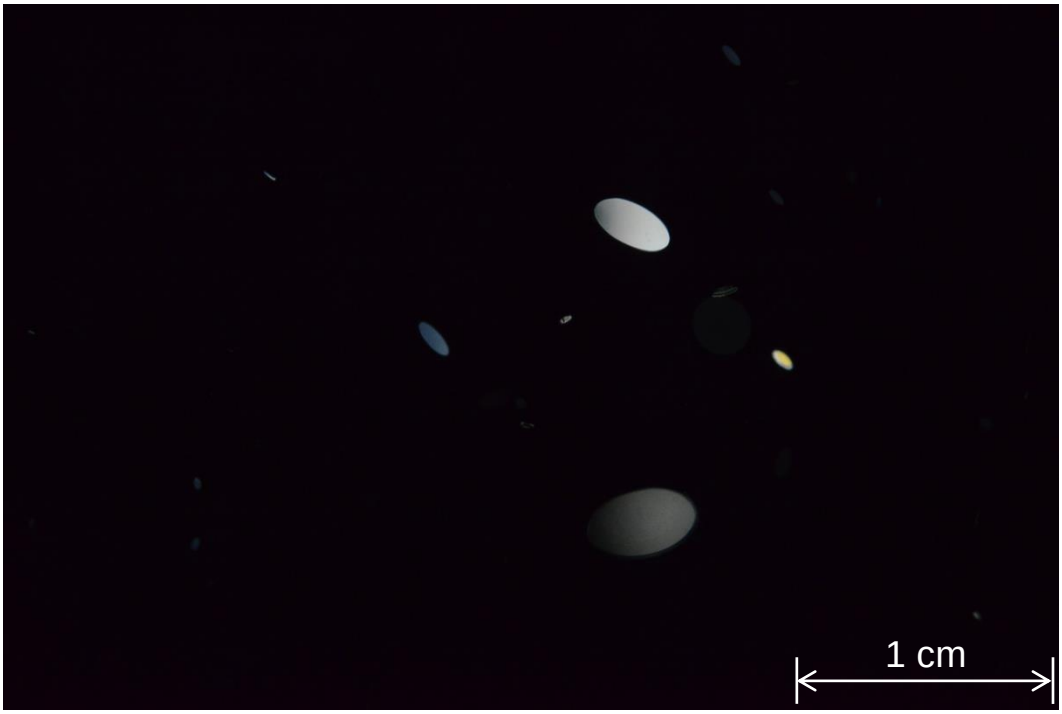

Figure 1-1: Suspended frazil ice particles.

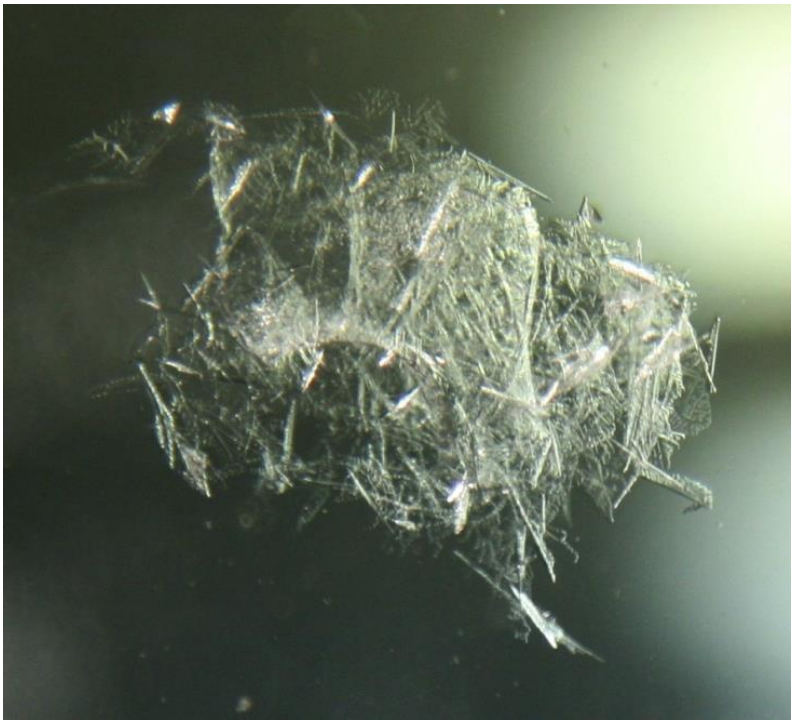

Figure 1-2: A frazil floc (photo courtesy of T. Ghobrial).

Figure 1-3: Frazil pans (photo courtesy of F. Hicks).

Figure 1-4: Bridging – flow direction is indicated by the white arrow (photo courtesy of M. Loewen).

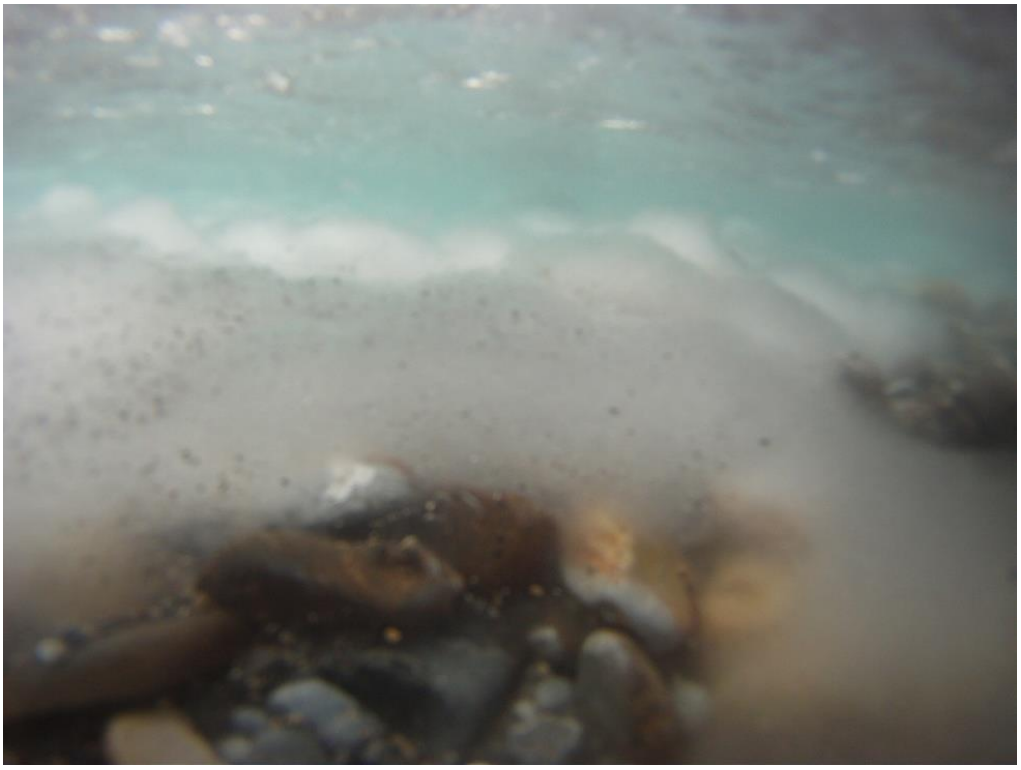

Figure 1-5: Anchor ice (photo courtesy of S. Emmer).

Figure 1-6: Skim ice (photo courtesy of M. Loewen).

References

Brown, R. S., Hubert, W. A., and Daly, S. F. (2011). "A Primer on Winter, Ice, and Fish: What Fisheries Biologists Should Know about Winter Ice Processes and Stream-Dwelling Fish." *Fisheries*, 36(1), 8–26.

Clark, S., and Doering, J. (2006). "Laboratory Experiments on Frazil-Size Characteristics in a Counterrotating Flume." *Journal of Hydraulic Engineering*, American Society of Civil Engineers, 132(1), 94–101.

Clark, S., and Doering, J. (2008). "Experimental investigation of the effects of turbulence intensity on frazil ice characteristics." *Canadian Journal of Civil Engineering*, 35(1), 67–79.

Daly, S. F., and Colbeck, S. C. (1986). "Frazil ice measurements in CRREL's flume facility." *Proceedings of the IAHR Ice Symposium 1986*, International Association for Hydraulic Research, Iowa City, Iowa, USA, 427–438.

Doering, J. C., and Morris, M. P. (2003). "A digital image processing system to characterize frazil ice." *Canadian Journal of Civil Engineering*, Canadian Science Publishing, 30(1), 1.

Ghobrial, T. R., Loewen, M. R., and Hicks, F. E. (2013a). "Continuous monitoring of river surface ice during freeze-up using upward looking sonar." *Cold Regions Science and Technology*, Elsevier B.V., 86, 69–85.

Ghobrial, T. R., Loewen, M. R., and Hicks, F. E. (2013b). "Characterizing suspended frazil ice in rivers using upward looking sonars." *Cold Regions Science and Technology*, Elsevier B.V., 86, 113–126.

Gosink, J. P., and Osterkamp, T. E. (1983). "Measurements and Analyses of Velocity Profiles and Frazil Ice-Crystal Rise Velocities during periods of Frazil-Ice Formation in Rivers." *Annals of Glaciology*, 79–84.

Marko, J. R., and Jasek, M. (2010a). "Sonar detection and measurements of ice in a freezing river I: Methods and data characteristics." *Cold Regions Science and Technology*.

Marko, J. R., and Jasek, M. (2010b). "Sonar detection and measurement of ice in a freezing river II: Observations and results on frazil ice." *Cold Regions Science and Technology*.

Matoušek, V. (1992). "Frazil and skim ice formation in rivers." *Proceedings of the 11th International Symposium on Ice*, International Association for Hydraulic Engineering & Research, Banff, Alberta, 1–22.

Morse, B., and Richard, M. (2009). “A field study of suspended frazil ice particles.” *Cold Regions Science and Technology*, Elsevier B.V., 55(1), 86–102.

Richard, M., and Morse, B. (2008). “Multiple frazil ice blockages at a water intake in the St. Lawrence River.” *Cold Regions Science and Technology*, 53(2), 131–149.

Stickler, M., Alfredsen, K. T., Linnansaari, T., and Fjeldstad, H. (2010). “The influence of dynamic ice formation on hydraulic heterogeneity in steep streams.” *River Research and Applications*, 26, 1187–1197.

Wuebben, J. L. (1984). “The Rise Pattern and Velocity of Frazil Ice.” *Proceedings of the 3rd Workshop on the Hydraulics of Ice Covered Rivers*, Committee on River Ice Processes and the Environment, Fredericton, New Brunswick, Canada, 297–316.

Chapter 2: Laboratory Experiments to determine Frazil Ice Properties[1]

2.1 Introduction

Frazil ice particles form in the turbulent flow zones of northern rivers during the early freeze-up period after the water temperature supercools to a few one hundredths of a degree below zero. Frazil particles in supercooled water readily adhere to each other; therefore, as the suspended frazil ice concentrations increase, the frazil particles will begin to flocculate together. When these slushy frazil flocs become sufficiently large for the buoyancy force to overcome fluid turbulence, they rise to the surface. The exposed surface of the floating slush freezes into a hard crust, forming frazil pans. Frazil pans, in turn, combine to form surface ice accumulations. Once the ice cover forms, the water can no longer supercool, and individual frazil particles become 'inactive' (i.e. they lose their adhesive nature). In addition to adhering to each other, 'active' frazil particles will also adhere to almost anything else they come in contact with including substrate material (sand, gravel, and cobbles) and aquatic vegetation. Large accumulations of frazil can cause major problems for facilities that require a continuous supply of freshwater, as the trash racks on the intakes may become blocked and bring any operations relying on the intake to a halt (Clark and Doering 2006).

---

[1] A version of this chapter has been published. McFarlane, V., Loewen, M., Hicks, F., 2012. Proceedings of the Annual Conference and General Meeting of the CSCE - 2012. Edmonton, Alberta, pp. 1–10.

At present, there is no practical means of measuring suspended frazil concentrations in the field. As a result very little is known about the flocculation process or the rise velocities of frazil particles, and highly empirical approaches are used to numerically model these processes. Recently however, upward looking sonars have been shown to be capable of detecting suspended frazil ice particles, and recent research suggests that it may be possible to quantitatively measure suspended frazil concentrations in the field using sonars as well (Ghobrial et al. 2012; Marko and Jasek 2010a; b). However, quantitative interpretation of sonar data requires knowledge of the shapes and size distributions of frazil particles and, therefore, that was the focus of this experimental study.

A number of previous experiments have been conducted to investigate the size distribution of in situ frazil ice particles. Daly and Colbeck (1986) used a "crystal imaging system" consisting of a 35 mm camera and a microscope to photograph frazil particles as they were generated in a 36.6 m long flume. Although these images were of high enough resolution to distinguish particles as small as 35 μm, no particles larger than ~0.5 mm in diameter were seen. For the particles that were measured, however, it was found that a lognormal distribution fit the data quite well. A digital imaging system was used to photograph frazil particles as they were generated in a counter-rotating flume by Doering and Morris (2003) and Clark and Doering (2006, 2004). The images were cross polarized to remove

background noise and processed using a Matlab program. Particles as large as 5 mm in diameter were measured by Clark and Doering (2006), however the pixel size for these images was 55 μm. It was assumed that an object must be at least 3 pixels in the images to be classified as a frazil particle due to uncertainty caused by background noise, meaning that the smallest particles observed were 165 μm. Similar to Daly and Colbeck (1986), it was noted that a lognormal distribution was a good fit to the observed particle size distributions.

In this study, a new experimental apparatus and imaging system were used to measure a full range of frazil particle sizes (i.e. as small as those seen by Daly and Colbeck (1986) and as large as those observed by Clark and Doering (2006)). These experiments were conducted using a frazil ice production tank that generates turbulence while the water cools. Similar to Clark and Doering (2006), the images were cross polarized and then analyzed using a Matlab code. In this study a high resolution digital camera was used to minimize the size of each pixel making it possible to photograph particles as small as 35 μm, as reported by Daly and Colbeck (1986). The objectives of these experiments were to develop and verify a new image acquisition system and image processing algorithm, and to study the size distribution of frazil ice particles.

2.2 Experimental Setup

Experiments were performed using a frazil ice tank designed and constructed in the University of Alberta Civil Engineering Cold Room Facility. The tank is 0.8 m wide, 1.2 m long and 1.5 m deep, with the two 1.2 m by 1.5 m walls

constructed out of 19 mm thick tempered glass (Ghobrial et al. 2009). 6 mm thick stainless steel plate was used for the other two walls and the bottom of the tank, where four plastic propellers powered by NEMA 34 DC variable speed electric motors (1/3 H.P., 13.4 in.-lbs. of torque, max speed 1750 rpm) are used to generate turbulence (Ghobrial et al. 2009). A Sea-Bird SBE 39 Temperature and Pressure Recorder (accuracy ± 0.002^{o}C for temperature, 0.05% of full scale range for pressure) was used to monitor the water temperature during the experiments. It was connected to a computer located outside the cold room allowing for real time monitoring of the water temperature and the degree of supercooling.

Two arrays of 24 LED lights were mounted against the back wall of the tank and diffused by a 1.5 mm thick sheet of Teflon (Figure 2-1). This light passed through two Cavision 4x4" glass linear polarizing filters that were mounted 22 mm apart, rotated at 90 degrees to each other and suspended in the tank flush to the front wall. Any light passing through the filters was cross-polarized, which has the effect of producing an image with a black background in which only ice particles that pass between the filters and refract the light could be seen. A Nikon D3 digital single-lens reflex (DSLR) camera equipped with a Kenko 25 mm Uniplus Tube DG extension ring and an AF Micro-Nikkor 60 mm f/2.8D lens was used to capture the images. The camera was mounted on a tripod 55 mm away from the front wall of the tank and focused on a plane approximately half way between the two polarizing filters (Figure 2-2).

During each experiment, 12 megapixel (4256x2832 pixel) resolution JPEG images were taken using the following camera settings: ISO 6400, shutter speed 1/2000 s, and aperture of f/25. It was determined during preliminary experiments that these settings provided the optimal image clarity and brightness.

2.3 Experimental Procedure

The cold room and water temperatures were held at 2^{o}C between experiments to ensure that any residual ice from previous experiments had melted. To begin each experiment the polarizers were mounted in the tank and the propellers were turned on and set to a speed of 320 rpm, which maximized the amount of turbulence in the water without entraining air at the surface. The Sea-Bird was mounted in the tank, connected to the computer, and setup to acquire a sample every 1.5 seconds for the duration of the experiment. The clocks in the Sea-Bird and the camera were synchronized to the computer to ensure that the image, temperature, and pressure data were all sampled with a common time base. At this point the temperature in the cold room was reduced to -10^{o}C.

Next, the ISO, shutter speed, and aperture settings on the camera were all set to the predetermined values as outlined above. The camera was then taken into the cold room and mounted on the tripod. The camera could not be left in the cold room between experiments because frost would form on the lens and the battery would drain rapidly. The LED lights were turned on and all other lights in the cold room were switched off to maximize the contrast in the images. A clear plastic ruler was then lowered midway between the polarizing filters and the lens

was manually focused on it. Test images were then taken with the ruler held against the front and rear polarizers to check that the images were in focus across the entire measuring volume. The images with the ruler at the front and rear of the measuring volume would later be used as "scale images" to determine the pixel size (mm/pixel) of the images; the pixel size at the front and rear were determined in Matlab by measuring the number of pixels spanning a known length, and then averaged to determine the mean pixel size. A series of background images were then taken while there was still no frazil ice in the tank. These images were averaged and subtracted from the frazil ice images during processing to remove any error due to imperfections in the glass, spots on the lens, or background light that passed through the filters.

Once the water temperature reached 0^{o}C the image acquisition was started. Images were taken at a frequency of 1 Hz for the next 16 minutes and 39 seconds. A total of 999 images were acquired, which was the maximum number of images the auto timer on the camera could be set to record. By the end of the image acquisition period, frazil production had ceased and most of the particles had flocculated and risen to the surface. The camera was then removed from the cold room and the room temperature was set to 2^{o}C to allow the ice to melt in preparation for the next experiment.

2.4 Analysis of Data

Two overlapping series of 260 images were extracted for analysis: the first series began just before the first frazil particles were observed and ended when the

particles began to flocculate, while the second series began 130 seconds later than the first series when frazil concentrations were high and ended when many of the particles had flocculated. Both image series were then analyzed using a digital image processing algorithm written in Matlab similar to that described by Clark and Doering (2006). The analysis of each image was performed using the following steps: pre-processing, particle detection, and particle analysis & validation.

2.4.1 *Pre-Processing*

First a set of ten background images was averaged. A raw frazil image was then loaded (Figure 2-3a) and the average background image was subtracted from it. The resulting image was then converted to grayscale, and subsequently to two binary images, first using a high threshold (Figure 2-3b) and second using a low threshold (Figure 2-3c). These two binary images would be compared to each other to determine the extent of each particle later in the analysis process.

2.4.2 *Particle Detection*

The high threshold image was then dilated and compared to the low threshold image to determine the extent of each particle and fill any dark "holes" in a particle that were visible in the high threshold image. Following dilation, the algorithm checked to determine if any pixel converted to a one in the high threshold image was also a one in the low threshold image. If so its value remained one, otherwise it reverted to zero. This process was used instead of a simple dilation-erosion procedure because it dilates outward from very bright pixels only, which typically correspond to frazil particles, and ignores background

noise or specks in the image (Clark and Doering 2006). This procedure was repeated until none of the particles were changing in size between iterations (Figure 2-3d).

2.4.3 *Particle Analysis & Validation*

Each particle (defined as a contiguous group of ones in the binary image) was then identified and analyzed. The area and perimeter in pixels of each identified particle were computed and two criteria were applied to improve the accuracy of the measurements. First, particles with a major axis length less than 3 pixels were discarded. This was because particles this small tend to be indistinguishable from background noise (Clark and Doering 2006). Second, the shape of the imaged particles was compared to the expected shape of frazil ice particles. The frazil particles generated in the tank are predominately disc shaped, and therefore they should appear in the images as a circle, an ellipse, or a straight line depending on their angle relative to the image plane. This criterion was applied by comparing the shape of each particle to that of a fitted ellipse.

First the normalized second central moments of each particle were calculated. These were then used to compute the major and minor axes lengths of an ellipse with the same normalized second central moments as the particle. Next, the major and minor axes lengths were used to calculate the area and perimeter of the fitted ellipse. For each particle, the actual area and perimeter were then compared to those of the fitted ellipse. If the actual area was less than 85% of the ellipse area, or if the percent difference between the particle perimeter and ellipse

perimeter was greater than 25%, the particle was discarded. These thresholds were determined by trial-and-error and visual inspection of images (e.g. Figure 2-3d) to confirm that oddly shaped particles were discarded. The accuracy of this method was determined by visually examining a total of 480 particles observed in the raw images and checking to see if they were accepted or rejected by the algorithm. It was found that only 15 (3.125%) of them were incorrectly retained when they should have been discarded (false positives), while only 6 (1.25%) of them were incorrectly discarded when they should have been retained (false negatives), demonstrating that this method correctly identifies frazil ice particles in the images 95% of the time. Particles that were discarded were typically jagged in shape or may have been disc shaped but their orientation caused them to appear as curved lines in the processed images (see Figure 2-3d). The size of each remaining particle was assumed to be equal to the major axis length of the fitted ellipse.

After all of the images had been processed in the manner described above, the mean, mode, median, and standard deviation of the particle sizes were calculated for the entire image series and histograms of particle sizes were generated.

2.5 Results and Discussion

Three separate experiments performed under the same conditions on June 28, July 26, and July 29, 2011 were analyzed. For the first image series analyzed in each of these experiments a total of 660, 1060, and 1234 particles were identified with mean diameters of 0.81, 0.76, and 0.84 mm and standard deviations of 0.59, 0.55, and 0.56 mm respectively. Levene's test for equality of variances

(NIST/SEMATECH 2010) was then used to check the statistical similarity of the processed data from the three different experiments. This particular test was chosen because it is reported to work well for non-normally distributed data (NIST/SEMATECH 2010). The null hypothesis for Levene's test is that the variances are equal, and this is checked by comparing the "Levene test statistic" to the upper critical value of the F-distribution for a chosen significance level, α. The P-value of the data is also computed, and again the null hypothesis is rejected if the P-value is greater than α (NIST/SEMATECH 2010). After comparing the three experiments in this way it was found that they were statistically similar at the 5% significance level, and the cumulative data had a mean particle size of 0.80 mm and a standard deviation of 0.56 mm for a total of 2954 particles.

For the second image series analyzed in each experiment the number of particles identified was significantly higher, with counts of 5001, 4728, and 6028 for the June 28, July 26, and July 29 experiments, respectively. The mean diameter was 0.72 mm for all three experiments with standard deviations of 0.48, 0.47, and 0.47 mm, respectively. Levene's test was again performed and the three data sets were found to be statistically similar at the 5% significance level. The cumulative data had a mean particle diameter of 0.72 mm and a standard deviation of 0.47 mm for a total of 15757 particles, which is ~10% smaller than the mean diameter in the earlier time series. Most of the flocculated particles did not appear in the images because they had either risen to the surface or the flocs were too large to pass in between the polarizers. Those that did appear in the images were discarded based

on the comparison to a fitted ellipse because the flocs typically have an irregular shape.

The two combined size distributions from the three experiments are plotted in Figures 2-4 and 2-5. It was observed that a log-normal distribution, which has been suggested by Daly and Colbeck (1986), Clark and Doering (2004), and Clark and Doering (2006) to describe the size distribution of frazil particles, was a good fit to the data from both series of images. The smallest particles previously measured using a digital imaging technique were 165 μm (Clark and Doering 2006). Here, the use of a higher resolution digital camera and a smaller field of view allowed for the measurement of particles as small as 38.9 μm in diameter, which is of the same order as the 35 μm particles observed by Daly and Colbeck (1986). The largest particle observed was 5.08 mm in diameter which is in the same range as the largest particles photographed by Clark and Doering (2006).

2.6 Conclusions

The results from three experiments conducted in the frazil ice tank demonstrated that the digital image acquisition technique and the image processing algorithm provide accurate measurements of the size distribution of frazil ice particles. Particles from 39 μm to 5 mm in diameter were observed. It was also seen that a log-normal distribution was a good fit to the observed size distributions. Prior to flocculation a total of 2954 particles were identified in three experiments, with a mean diameter of 0.80 mm and standard deviation of 0.56 mm. A second image series that included images taken after flocculation began revealed 15757 particles

with a mean of 0.72 mm and standard deviation of 0.47 mm. This demonstrated that the technique remains effective even when flocculation occurs.

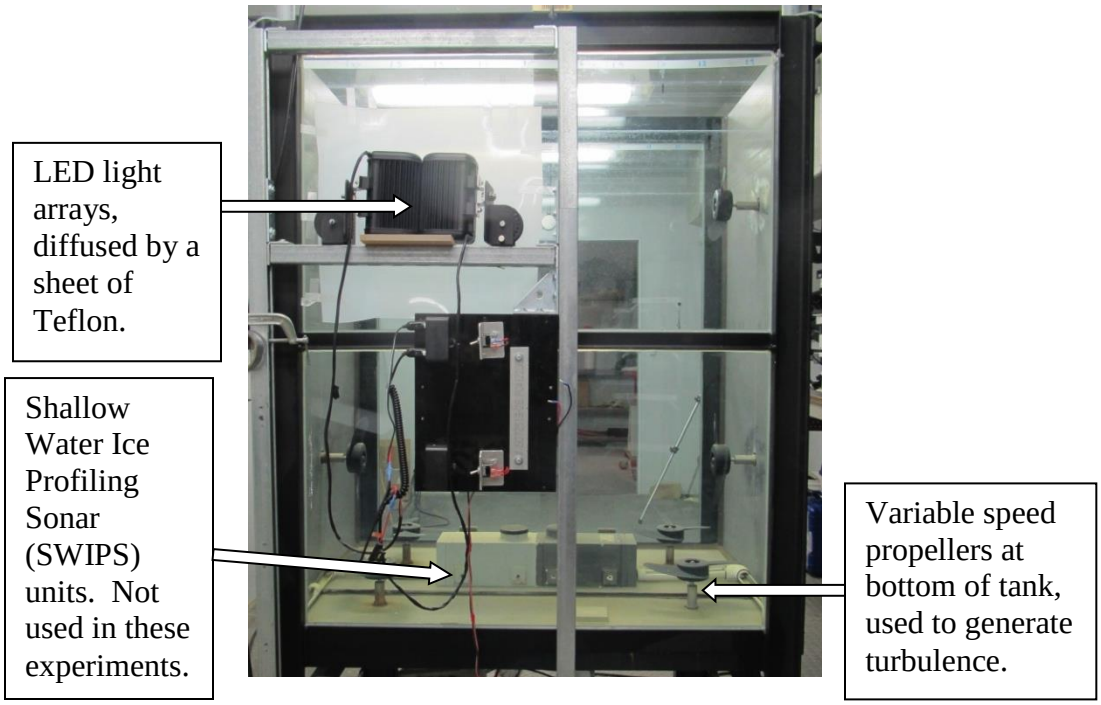

Figure 2-1: Rear view of the frazil ice production tank equipped with LED light arrays diffused by a sheet of Teflon.

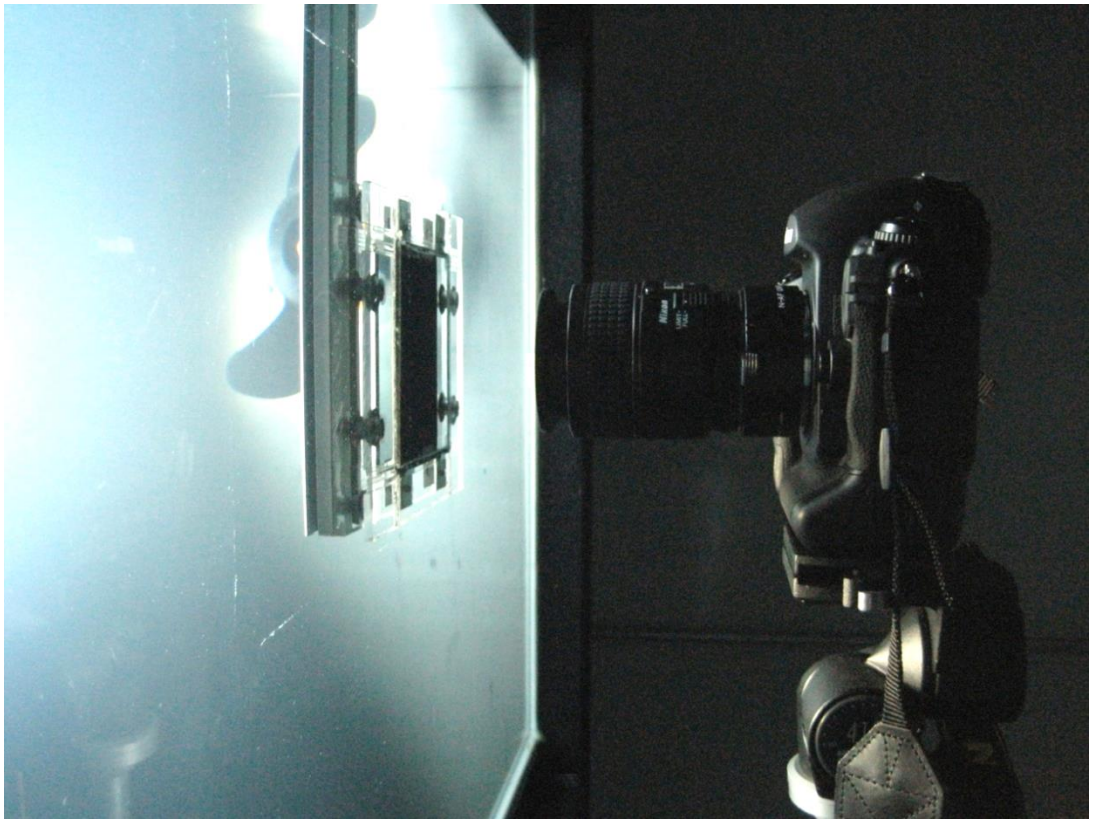

Figure 2-2: Camera mounted on tripod with the lens 55 mm from the tank wall. The polarising filters are seen mounted inside the tank.

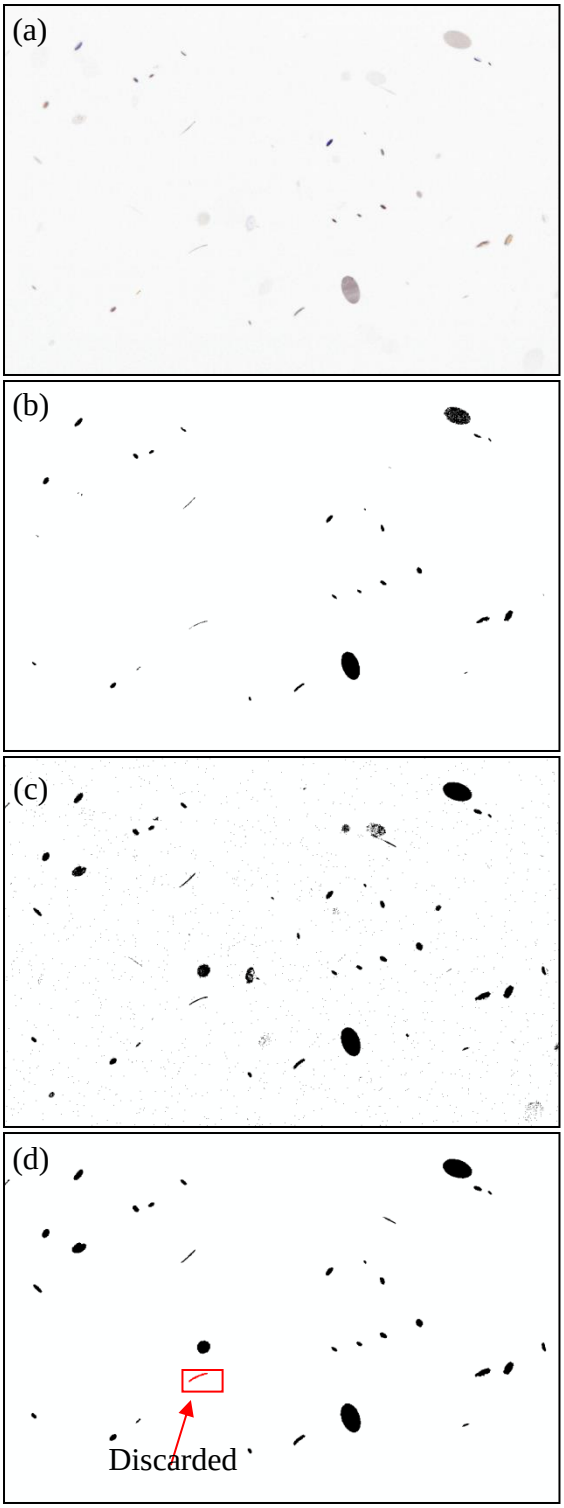

Figure 2-3: Image at different stages of processing (note that these are negative images with black and white reversed for clarity in this figure). (a) Raw image, (b) High threshold binary image, (c) Low threshold binary image, (d) Final binary image. Highlighted particle was discarded based on the fitted ellipse.

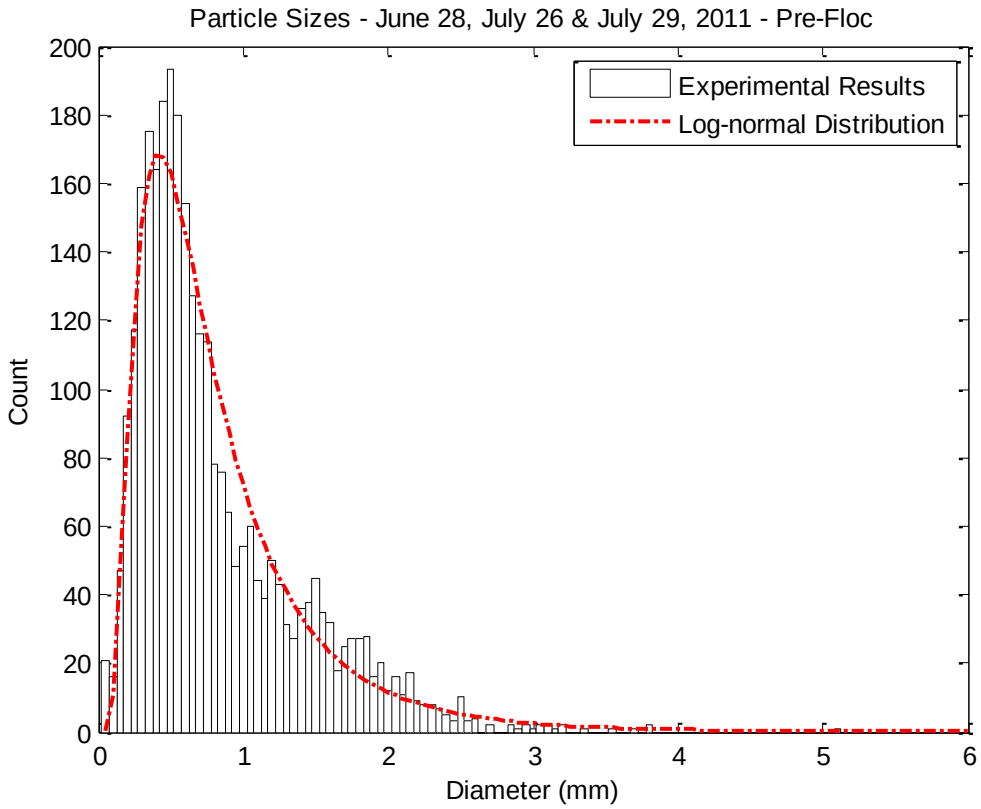

Figure 2-4: Frazil ice particle size distribution prior to flocculation, fitted with a log-normal distribution. The bin size is 0.05 mm.

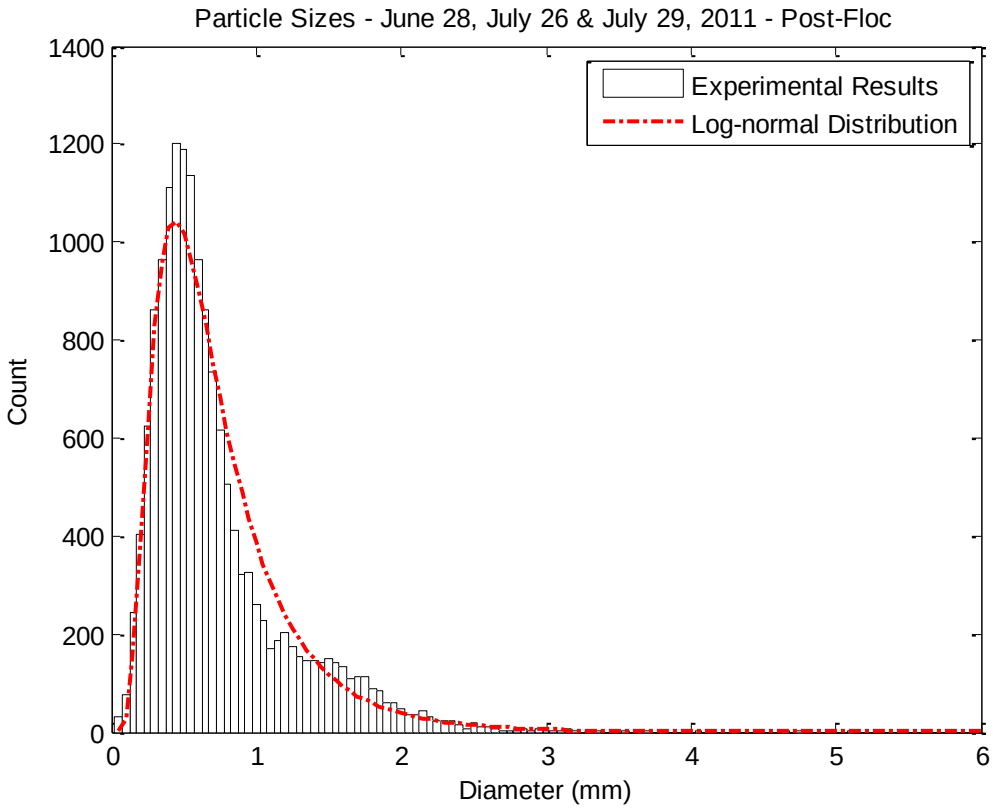

Figure 2-5: Frazil ice particle size distribution after flocculation, fitted with a lognormal distribution. The bin size is 0.05 mm.

References

Clark, S., and Doering, J. (2006). "Laboratory Experiments on Frazil-Size Characteristics in a Counterrotating Flume." *Journal of Hydraulic Engineering*, American Society of Civil Engineers, 132(1), 94–101.

Clark, S., and Doering, J. C. (2004). "A laboratory study of frazil ice size distributions." *Proceedings of the 17th International Symposium on Ice*, International Association of Hydraulic Engineering and Research, Saint Petersburg, Russia, 291–297.

Daly, S. F., and Colbeck, S. C. (1986). "Frazil ice measurements in CRREL's flume facility." *Proceedings of the IAHR Ice Symposium 1986*, International Association for Hydraulic Research, Iowa City, Iowa, USA, 427–438.

Doering, J. C., and Morris, M. P. (2003). "A digital image processing system to characterize frazil ice." *Canadian Journal of Civil Engineering*, Canadian Science Publishing, 30(1), 1.

Ghobrial, T., Loewen, M., and Hicks, F. (2009). "Frazil Ice Measurements Using the Shallow Water Ice Profiling Sonar." *15th Workshop on River Ice*, CGU HS Committee on River Ice Processes and the Environment, St. John's, Newfoundland and Labrador.

Ghobrial, T. R., Loewen, M. R., and Hicks, F. (2012). "Laboratory calibration of upward looking sonars for measuring suspended frazil ice concentration." *Cold Regions Science & Technology*, 70, 19–31.

Marko, J. R., and Jasek, M. (2010a). "Sonar detection and measurements of ice in a freezing river I: Methods and data characteristics." *Cold Regions Science and Technology*.

Marko, J. R., and Jasek, M. (2010b). "Sonar detection and measurement of ice in a freezing river II: Observations and results on frazil ice." *Cold Regions Science and Technology*.

NIST/SEMATECH. (2010). "NIST/SEMATECH e-Handbook of Statistical Methods."

Chapter 3: Laboratory Measurements of the Rise Velocity of Frazil Ice Particles[2]

3.1 Introduction

Formation of a river ice cover is influenced by many variables, but not all of them are fully understood. For example, it is well known that water will become supercooled near the water surface when the air temperature drops below zero prior to freeze-up, leading to the formation of small ice particles on the surface. In calm waters these particles will grow quickly at the surface leading to the formation of a skim ice cover or, if the velocity is high enough, a skim ice run (Clark, 2013). However, if the vertical component of the river turbulence is strong enough to overcome the buoyancy of these surface particles they will become entrained in the flow and the supercooling will extend to greater depths, allowing these particles to seed the growth of frazil ice crystals (Matoušek, 1992). Similarly, these disc shaped frazil particles will only remain entrained in the flow as long as the river turbulence can overcome the frazil rise velocity, and if the individual frazil particles remain entrained and reach high concentrations, they will accumulate together to form slushy frazil ice flocs, which in turn will rise to the surface and become frazil pans and rafts.

[2] A version of this chapter has been submitted for publication in Cold Regions Science and Technology with the authorship McFarlane, V., Loewen, M., and Hicks, F.

In order to predict whether skim ice, frazil ice, or some combination of the two will dominate the early freeze-up stages along a particular body of water, it is important to better understand the physics of rising frazil ice particles. Similar to the study of sediment transport, a logical place to start is with the rise velocity of these particles in quiescent water, which has been suggested by Matoušek (1992) to be a key variable in determining whether or not skim ice will form. The focus of this research was to provide such data for individual frazil particles of varying sizes. A specially designed tank located in the University of Alberta's Civil Engineering Cold Room Facility produced frazil ice particles in turbulent, supercooled water, and high-resolution digital images were captured of these particles as they passed between two polarising filters. Using an image processing algorithm each particle was identified and its diameter was determined, and the movement of the particle was then tracked to determine the rise velocity. A detailed description of the laboratory procedure and image processing algorithm is presented, the data is compared to existing theoretical solutions for the rise of frazil ice particles, and a new expression is derived to represent the rise velocity of vertically oriented discs in quiescent water.

3.2 Literature Review

Measuring the rise velocity of frazil ice particles is challenging and, as a result, few researchers have attempted these types of measurements to date. Gosink and Osterkamp (1983) used a stopwatch to time the rise of frazil ice particles that had been scooped out of the Chatanika River in Alaska with a graduated cylinder and found that the rise velocity generally increased with frazil particle diameter.

However, particle diameters were only measured to the nearest 0.5 mm (approximately) using the graduations on the cylinder for scale. Gosink and Osterkamp (1983) also noted that their measurements may have been impacted by residual turbulent motions, and that acceleration of small discs in the wake of larger discs was occasionally observed. They also included a number of data points, labelled as lab data, in their plot of rise velocity versus particle diameter, but did not provide any details of these laboratory experiments. Based on their observations, and assuming a simple force balance between the form drag and the buoyant force acting on a horizontal disc, Gosink and Osterkamp (1983) derived the following equation to predict a particle's rise velocity:

$$\rho_i \pi \left(\frac{d^2}{4}\right) ta = (\rho_w - \rho_i)\pi \left(\frac{d^2}{4}\right) tg - \left(\frac{\rho_w C_D V^2}{2}\right)\left(\frac{\pi d^2}{4}\right) \quad [1]$$

where ρ_i and ρ_w are the densities of ice and water, 920 and 1000 kg/m^3, respectively; d is the frazil particle diameter (m); t is the frazil particle thickness (m); a is the acceleration of the particle (m/s^2); g is the acceleration due to gravity (9.806 m/s^2); and C_D is the drag coefficient. Then, assuming that the acceleration of the particles was negligible (i.e. that each particle had reached its terminal rise velocity), equation [1] was rearranged to give the steady-state rise velocity of a horizontal frazil particle as follows:

$$V = \sqrt{2g't / C_D} \quad [2]$$

where g' is the reduced gravitational acceleration, given by $g' = g(\rho_w - \rho_i)/\rho_w$. In order to estimate C_D, Gosink and Osterkamp (1983) used data reported by Willmarth et al. (1964) and Schlichting (1968) to derive the following empirical equation relating the drag coefficient of a disc to the Reynolds number:

$$\log C_D = 1.386 - 0.892 \log Re + 0.111 (\log Re)^2 \qquad [3]$$

where $Re = Vd/v$ is the Reynolds number, v is the kinematic viscosity of water at 0°C (1.8×10^{-6} m^2/s), and equation [3] is valid for $Re < 100$. Equations [2] and [3] were then solved for different ratios of d/t, or 'aspect ratios', and used to plot theoretical rise velocity versus particle diameter curves. Gosink and Osterkamp (1983) found that their data was enveloped by curves for aspect ratios of 10 and 50, and ultimately recommended an aspect ratio of about 20 to represent all frazil particles.

Using a procedure similar to that of Gosink and Osterkamp (1983), Wuebben (1984) also attempted to experimentally measure frazil ice rise velocities while working in a laboratory setting. Although he did not describe how the frazil ice particles were produced, Wuebben (1984) does describe how he timed particles with a stopwatch and estimated their diameters to the nearest 0.25 mm through visual comparison to a scale as they ascended in a one litre graduated cylinder. After plotting the observed rise velocities as a function of particle diameter, Wuebben (1984) suggested the following power law relationship:

$$V = 0.019d^{2/3} \approx 0.02d^{2/3} \quad [4]$$

Wuebben (1984) noted that, aside from equation [4] having the desirable property of passing through the origin, there was no strong justification for selecting any particular relationship due to the scatter in the limited data that was available. Wuebben (1984) also fit a similar curve to the data reported by Gosink and Osterkamp (1983), and found the relationship:

$$V = 0.3751d^{0.64} \approx 0.45d^{2/3} \quad [5]$$

He speculated that the difference between equations [4] and [5] could possibly be due to differing particle aspect ratios brought on by different nucleation and growth conditions, since most of Gosink and Osterkamp's (1983) particles were produced in a river, while Wuebben's (1984) experiments were conducted in a laboratory environment. Assuming Stokes flow Wuebben (1984) derived the following theoretical equation for the rise velocity:

$$V = \frac{g'td}{10.2\nu} \quad [6]$$

However, he noted that because the Reynolds number is typically greater than one for frazil ice particles, Stokes flow is likely not a good assumption. Each of the solutions presented by Gosink and Osterkamp (1983) and Wuebben (1984) along with their rise velocity data are plotted in Figure 3-1.

In addition to equations [2] to [6], a number of other equations exist for predicting the rise velocity of frazil ice and they are summarised nicely by Morse and Richard (2009). Shulyakovskii (1960) (as reported by Zakharov et al. (1972)) provided one such relationship, taking into account the kinematic viscosity of water as well as the particle diameter, and provided the equation:

$$V = \left(4.006 \times 10^{5}\right) \nu \, d^{0.69} \qquad [7]$$

Ashton (1983) assumed that the rising frazil ice particles would fall in the Stokes range (i.e. $Re << 1$) and derived the following equation:

$$V = \frac{g' d_e^2}{18 K_r \nu} \qquad [8]$$

where d_e is the equivalent diameter of a sphere with the same volume as the frazil disc (m), and K_r is a constant resistance factor, estimated by Hammar and Shen (1991) to be $K_r = 2$.

Daly (1984) noted that for a disc with its major axis perpendicular to the flow, the drag coefficient is a function of Reynolds number (equation [3]) and is therefore related to the particle diameter. Bearing the Re-C_d relationship in mind, a series of equations were provided by Daly (1984) applicable to different ranges of particle

diameters and thus different levels of turbulence and varying drag coefficients. The equations are:

$$V = 0.02\left(g'_D \nu^{-1} d^2\right) \quad \text{for } d < 0.0006 \text{ m (Stokes range)} \qquad [9]$$

$$V = 0.0726\left(g'^{\,0.715}_D \nu^{-0.428} d^{1.14}\right) \quad \text{for } 0.0006 \text{ m} < d < 0.0028 \text{ m (intermediate range)} \qquad [10]$$

$$V = \frac{1}{2}\left(g'_D\, d\right)^{1/2} \quad \text{for } d \geq 0.0028 \text{ m (fully turbulent range)} \qquad [11]$$

where the reduced gravity, g'_D, is defined as:

$$g'_D = 2\left(\frac{\rho_w - \rho_i}{\rho_w}\right)\left(\frac{gK_v}{\pi}\right) \qquad [12]$$

and K_v, the volumetric shape factor, is calculated based on the particle volume, $\forall$, as follows:

$$K_v = \frac{8\forall}{d^3} \qquad [13]$$

Matoušek (1992) carried out experiments using discs made of polyethylene to approximate frazil ice particles, noting that polyethylene has the same density of ice and should therefore model the behaviour of ice particles accurately. Although Matoušek (1992) did not specify the exact density of the polyethylene

he used, it has since been used to approximate ice in other studies (e.g. Healy and Hicks (2007)) who mention the density of polyethylene to be 920 kg/m^3. Matoušek (1992) measured the rise velocities of polyethylene discs with diameters of two, four, and 5.5 mm and thicknesses ranging from 0.03 to 0.27 mm, and used this data to derive the following empirical equation:

$$V = 1.31 \times 10^{-5} \frac{d^{0.29} t^{0.61}}{\nu} \qquad [14]$$

Svensson and Omstedt (1994) simplified Daly's (1984) equations into the following single representative equation:

$$V = 32.8 d^{1.2} \qquad [15]$$

Another theoretical solution was derived using a modified version of Rubey's (1933) formula by Shen and Wang (1995), treating the suspended frazil particles in a similar manner to suspended sediment, giving the equation:

$$V = -4 \frac{k_2}{k_1} \frac{\nu}{d} + \sqrt{\left(4 \frac{k_2}{k_1} \frac{\nu}{d} \right)^2 + \frac{4}{3 k_1} \left(\frac{\rho_w - \rho_i}{\rho_w} \right) g d} \qquad [16]$$

where k_1 = 1.22 and k_2 = 4.27.

It is of note that each of these equations, with the exception of equation [3] from Gosink and Osterkamp (1983), equations [10] and [11] from Daly (1984), and equation [14] from Matoušek (1992) assume that the Stokes range approximation is valid. Morse and Richard (2009) concluded that this assumption was likely invalid as frazil ice particle Reynolds numbers are "generally far greater than unity". As an alternative, Morse and Richard (2009) simplified a number of equations derived by Khvorostyanov and Curry (2005, 2002) to describe the terminal velocities of atmospheric particles with Reynolds numbers less than 5000 into a form suitable for frazil ice particles with diameters less than 7 mm. The simplified equations are (in mm-s units):

$$V = 2.025d^{1.621} \quad \text{for } d \leq 1.27 \text{ mm} \qquad [17]$$

$$V = -0.103d^2 + 4.069d - 2.024 \quad \text{for } d > 1.27 \text{ mm} \qquad [18]$$

Each of these theoretical models are plotted in Figure 3-2, along with Gosink and Osterkamp's (1983) and Wuebben's (1984) data, and it can be seen that no single equation is a good fit to the entire data set.

Although studies of frazil rise velocities are rare, there have been a number of studies of falling disc shaped particles. For example, Willmarth et al. (1964) investigated the effect of Reynolds number on the characteristics of freely falling discs. They found that discs with very small particle Reynolds numbers (i.e. $Re \leq 1$) will continue to fall with whatever orientation they had when they began their

descent. However, for *Re* between approximately 1 and 100 they observed that a disc would stabilise with a horizontal orientation. This is important to note since the existing theoretical models for frazil rise all assume the disc is horizontal while it rises. Similarly, Zhong and Lee (2012) investigated falling thin plastic discs with diameters between 3 and 11 mm and Reynolds numbers ranging from 40 to 200. They observed a symmetric flow pattern and steady wake behind the discs for $40 < Re < 105$, indicating that the discs had a stable, horizontal orientation during their descent at these Reynolds numbers.

3.3 Experimental Setup

The measurements were conducted in a frazil ice tank is located in the University of Alberta's Civil Engineering Cold Room Facility. The tank is 0.8 m wide, 1.2 m long and 1.5 m deep (Figure 3-3a). The 1.2 m by 1.5 m walls are constructed out of 19 mm thick tempered glass, while the other two walls and bottom of the tank are made of 6 mm thick stainless steel plate. Turbulence was generated in the tank by four plastic propellers powered by NEMA 34 DC variable speed electric motors (278 watts, 1.514 N-m of torque, max speed 1750 rpm) that are mounted to the tank bottom (Ghobrial et al., 2009), and were set to speeds of 125 or 325 rpm for each experiment. A computer located outside of the cold room was connected to a Sea-Bird SBE 39 Temperature Recorder (accuracy ± 0.002°C) enabling real-time monitoring of the water temperature and the degree of supercooling during the experiments. Two 24-bulb arrays of Larson Electronics 3-watt LED lights were mounted against the back wall of the tank and diffused by a 1.5 mm thick piece of translucent plastic sheeting to backlight the images. Two

Cavision 10x10 cm glass linear polarizing filters mounted 22 mm apart were suspended in the tank flush to the glass wall opposite the lights, such that the centre of the measuring volume was 1.06 m above the bottom of the tank. The filters were oriented at 90° to each other causing the light passing through them to be cross-polarised, effectively producing a black background upon which only the ice particles (that refract the incident light) were visible, a technique first described for photographing frazil ice by Doering and Morris (2003).

A Nikon D800 digital single-lens reflex (DSLR) camera equipped with a Kenko 25 mm Uniplus Tube DG extension ring and an AF Micro-Nikkor 60 mm f/2.8D lens was used to capture digital images of rising frazil ice particles. The camera was mounted on a tripod such that the face of the lens, when fully retracted, was 55 mm away from, and parallel to, the front wall of the tank (Figure 3-3b). The lens was then focused on a plane approximately half way between the two polarizing filters. Images 4.1 ± 0.9 cm wide and 2.7 ± 0.6 cm tall with a resolution of 36 megapixels (7360 x 4912 pixels) were captured during each experiment using the following camera settings: an ISO of 6400, a shutter speed of 1/2000 s, and an aperture of f/25. These settings were found to provide the optimal balance of image clarity and brightness during preliminary experiments. The continuous high-speed shooting mode of the camera was used to acquire the rise velocity images. A series of time trials were conducted in which continuous high-speed photographs were taken of a digital timer and it was determined that

the camera captured an image every 0.247 seconds, with a standard deviation of 0.009 seconds, in this mode.

3.4 Experimental Procedure

The five rise velocity experiments presented were carried out at air temperatures of either -5 or -10 degrees Celsius (°C) and propeller speeds of 125 or 325 rpm, as detailed in Table 3-1, for the purpose of studying the impact of these variables on size distribution. At the beginning of an experiment the polarizers were mounted in the tank, the propellers were switched on, and the temperature recorder was programmed to record the water temperature once every 1.5 seconds for the duration of the experiment. The clocks in the temperature recorder and camera were synchronised with the computer being used for real time monitoring of the water temperature, to ensure that all data was recorded with a common time base. The temperature in the cold room was then reduced to either -5 or -10 °C and the water temperature decreased steadily for one to two hours depending on the initial temperature, until supercooling was achieved.

As the water temperature approached 0°C, the camera was programmed to the ISO, shutter speed, and aperture settings described above, taken into the cold room, and set up level on the tripod. This was done just five to ten minutes before the water temperature reached 0°C, otherwise frost would form on the lens. The LED lights were powered on, the camera focus was adjusted, and scale images were taken of a clear plastic ruler positioned first at the front and then at the back of the measuring volume. These two scales were later averaged to determine the

pixel size in the centre of the measuring volume, which ranged from 5.4 to 5.7 μm. Background images were then captured prior to the formation of the first ice particles to detect any imperfections in the glass, spots on the lens, or background light that had passed through the polarizing filters.

Once the water temperature dropped below 0°C, frazil production started and 999 images (the maximum number the camera could be automatically set to record) were taken at a frequency of one Hz to determine the size distribution of suspended frazil ice particles (McFarlane et al., 2012). After all of the suspended frazil images had been captured, the propellers were switched off and the residual turbulence in the water was allowed to dissipate for two to three minutes before acquisition of the rise velocity images commenced. The camera was then set to the continuous high-speed shooting mode and digital images of rising particles were then captured every 0.247 seconds as they passed between the polarizing filters. A series of 200 rise velocity images could be recorded before the memory buffer in the camera would fill up, at which point a break of a few seconds was required to back up the images to the memory card. For each experiment, three to five series of rise velocity images were taken in this manner until the majority of the frazil particles appeared to have reached the surface. The camera was then removed from the cold room and the air temperature was increased to 2°C, to melt the ice prior to the next experiment.

3.5 Data Analysis

3.5.1 *Digital Image Processing Algorithm*

The first stage of data analysis was performed using a digital image processing algorithm written in Matlab, similar to the one described by Clark and Doering (2006). Each frazil image was first pre-processed in preparation for detailed analysis. A series of 10 background images was averaged to create a single background image for the specific experiment; this was subtracted from each raw frazil image to remove any imperfections. The frazil image was next converted into two binary images – one using a high threshold and one using a low threshold. To ensure that only clear, bright frazil particles were analysed, the high threshold binary image – in which only pixels that were very bright in the raw image were visible – was used as the starting point for identifying particles. The high threshold image was dilated by one pixel (i.e. each pixel immediately surrounding a pixel that was a 1 was converted to a 1) and compared to the low threshold image. If a pixel converted to a 1 through dilation was found to be a 1 in the low threshold binary image as well, it was regarded as part of the particle and remained a 1. However, if the corresponding pixel in the low threshold image was a 0, then the dilated pixel in the high threshold image would revert to 0. This process was repeated until none of the particles were changing in size from one iteration to the next, and therefore the extents of each particle had been determined. Each particle was then dilated and subsequently eroded (the opposite of dilation) by four pixels to ensure that any possible 'holes' in the particle had been filled.

Each contiguous group of ones in the binary image was then identified as a potential particle using the Matlab command 'bwlabel' and analysed using the following procedure. First, as was suggested by Clark and Doering (2006), any particles with a major axis length equivalent to three or fewer pixels were discarded, as particles this small tended to be indistinguishable from background noise. All remaining particles were then checked to determine if they were discoid in shape. A disc shaped particle will appear as a circle, ellipse, or straight line in the images depending on its orientation relative to the image plane. This was tested by comparing the area and perimeter of each identified particle to those of a 'fitted ellipse' that was calculated by Matlab to have the same normalised second central moments as the particle of interest. If the actual area was less than 90% of the ellipse area, or if the percent difference between the particle perimeter and ellipse perimeter was greater than 25%, the particle was discarded. These thresholds were determined using a trial-and-error process in which particles identified as discs by the Matlab algorithm were compared to the raw images through visual inspection. A total of 957 potential particles were tested in this way and it was found that only 59 of them (6.2%) were incorrectly retained when they should have been discarded (false positives) while only 6 of them (0.6%) were incorrectly discarded (false negatives), demonstrating that this method correctly classified particles over 93% of the time. Discarded particles were typically jagged in shape or in some cases may have in fact been discs but the particle orientation, together with the way in which they caught the light, caused

them to appear as curved lines. The size of each retained particle was assumed to be equal to the major axis length of the fitted ellipse. In addition to the major axis length, the location of the particle centroid, in pixels, was also recorded.

3.5.2 *Measurement of Rise Velocity*

Particle rise velocities were determined by manually tracking the location of a particle's centroid, using the data computed by the Matlab algorithm, as it moved from one image to the next, and copying these values into a spreadsheet program. The image number that the particle was first visible in, the time at which that image was acquired, and the particle number in that image were also recorded along with the particle diameter. Rise velocities for each particle were calculated based on the total displacement in the vertical (y) direction, in pixels, between the first and last images in which the particle was visible, and the elapsed time between these images. Figures 3-4a and 3-4b present 50 superimposed images for experiments 40 and 49, respectively. The two plots illustrate the trajectories on which the observed particles were traveling, and the movement of the centroids of tracked particles are marked in yellow.

It was also necessary to determine whether or not residual currents in the tank were significantly affecting the particle rise velocities. In Figure 3-5 the rise velocity data is plotted as a function of the time since the propellers in the tank had been switched off, and the data points are grouped based on the particle diameter. It is evident from Figure 3-5 that faster particles were observed earlier, while only the smallest particles ($d < 0.50$ mm) were not observed over the entire

range of times. While the faster particles could potentially be caused by some residual current in the tank, this is unlikely as it can be seen in Figure 3-4 that the majority of the particles are rising on trajectories that were close to vertical regardless of how long it had been since the propellers had been switched off (2.5 minutes in Figure 3-4a, 5 minutes in Figure 3-4b). In Figure 3-6 an image showing particle trajectories from experiment 43 in which significant residual currents were present is presented. All of the particles visible in the image were rising at an angle of ~33^{o} from the vertical towards the upper left corner of the image. It is possible that some particles could rise at an angle depending on their orientation but that is clearly not the case in Figure 3-6 as the particles are seen to be rising with a number of different orientations. Due to the influence of residual currents in the tank the data from experiment 43 was not included in the final results.

A more likely explanation for why the higher velocities were all recorded less than four minutes after the propellers had been switched off is that the faster rising particles had simply risen above the field of view of the camera after approximately three minutes. Considering that the tank is only 1.5 metres deep and the polarizers were mounted such that the centre of the camera's field of view was located 1.06 m from the bottom of the tank, a particle traveling at a constant velocity of 10 mm/s, for example, would theoretically pass through the field of view after one minute and 46 seconds of rise if it had begun ascending from the tank bottom. In reality, it was observed that the particles continued to swirl for a

short while after the propellers had been switched off as the turbulent eddies in the tank dissipated, and only then began their ascent. As a result even a fast moving particle starting from the bottom of the tank could potentially take up to three minutes to reach the sample volume, which is approximately when the final particles with velocities greater than 5 mm/s are seen in Figure 3-5.

3.6 Results and Discussion

3.6.1 *Frazil Particle Characteristics*

In order to better understand the rise of frazil ice particles, knowledge of other particle properties such as diameter and thickness is very important. For this reason the size distribution of the suspended particles captured in the tank prior to each of the rise velocity experiments was determined. McFarlane et al. (2012) provides the details of those size determination experiments. An example histogram displaying the size distribution of suspended particles captured in one of the experiments is shown in Figure 3-7. It can be seen in this figure that a lognormal distribution fits the particle size data quite well, which has been suggested by other researchers such as Daly and Colbeck (1986) and Clark and Doering (2006, 2004). Overall, in the size distribution images captured prior to the rise velocity experiments presented, 11,102 suspended particles were analysed with a mean diameter of 0.86 mm.

Occasionally, particles were oriented in such a way that the particle thickness could be measured in the image. Four example images of particles in which the thickness was measured are shown in Figure 3-8. Thicknesses in the range of

0.03 to 0.12 mm with a mean and standard deviation of 0.07 mm and 0.02 mm, respectively, were estimated for 38 of these particles. The aspect ratios for these discs were found to range from 11 to 71 with a mean of 37 and a standard deviation of 11. The particle diameter is presented versus particle thickness in Figure 3-9, and there is no definitive relationship between the two dimensions, as is evidenced by the low R^2 value for the linear regression curve shown and the range of diameters observed for a single thickness. This supports the hypothesis that, rather than assuming a constant aspect ratio, it may be more realistic to assume that aspect ratio increases as the disks grow, due to preferential crystal growth normal to the *c*-axis (i.e. with increasing diameter). It is also important to note that the enveloping curves for aspect ratios of 10 and 50 suggested by Gosink and Osterkamp (1983) fall within this range. Daly (1994) provided an explanation for preferential growth in diameter rather than thickness, based on the theory that the roughness of the crystal face, described by the parameter α, will influence its growth rate. Any crystal face with an α value less than two was considered rough, while an α value greater than two indicated a smooth crystal surface. Fujioka (1978) (as referenced by Daly (1994)) determined that the α-value normal to the *c*-axis of a frazil crystal is 0.88, indicating a rough crystal face, and therefore concluded that crystal growth in this direction would be continuous and limited only by the rate of diffusion of latent heat. In the direction normal to the *a*-axis however (i.e. with increasing thickness), the α-value is 2.64, indicating a smooth crystal face and therefore a much slower growth rate in this direction.

3.6.2 *Experiment Results*

The rise velocities and diameters of the tracked particles ranged from 0.40 to 13.47 mm/s and 0.24 to 3.35 mm, respectively. The rise velocity of each particle is plotted as a function of particle diameter in Figure 3-10, and it is evident that there is a large amount of scatter in the data. Also shown in Figure 3-10 is the data presented by Gosink and Osterkamp (1983) and Wuebben (1984), and some of the relationships that they suggested. The first thing to notice in Figure 3-10 is that all of the data reported by Gosink and Osterkamp (1983) and Wuebben (1984) falls within the envelope of the data from this study. This may indicate that, although the particle diameters were only estimated and velocities were timed using a stopwatch, which could have caused noticeable error in the measurements, neither Gosink and Osterkamp's (1983) nor Wuebben's (1984) data set appears to be more correct nor incorrect than the other. It appears instead that they were unable to collect data for small, fast moving particles. Although it is not specified in their reports, this may be because of the limitations in the method that both Gosink and Osterkamp (1983) and Wuebben (1984) used for measuring and timing their particles, as it would be understandably easier to measure both the velocity and diameter of larger and/or slower moving particles. Also of note in this figure is that the solution to equations [2] and [3] for an aspect ratio of 10 passes through a large cluster of the current data in the 0.25 to 0.70 mm range. Equation [6] suggested by Wuebben (1984) for a constant thickness of 0.05 mm passes through this data as well, however this equation is only

applicable in the Stokes range. Neither of these curves appears to fit the data well beyond this point.

Enveloping curves were also determined for the current data using equations [2] and [3], and it was found that the curves corresponding to *d/t* values of 2 and 80 enveloped the data fairly well. However, based on the particle thickness and aspect ratio data presented in section 6.1 an aspect ratio of 2 seemed unrealistic. As an alternative to the assumption that a disc will rise with a perfectly horizontal orientation, the possibility of discs rising with a perfectly vertical orientation was also explored. When looking at the rise velocity images (Figure 3-4) it is clear that most discs are in fact oriented somewhere in between horizontal and vertical. For this study, the tracked particles were found to have values of *Re* ranged from 0.06 to 15.79, with an average value of 2.28 and standard deviation of 2.59. Of the 99 total particles, 41 had Reynolds numbers less than one. Knowing that discs with $Re < 1$ will not stabilise horizontally (Willmarth et al., 1964) it is reasonable to assume that many of these angled particles maintained that non-horizontal orientation during ascent, and also that the Stokes approximation may in fact be valid in some cases. Although the volume of the disc is the same and thus the buoyant force acting on it also does not change between the horizontal and vertical cases, the disc experiences less drag in the vertical orientation. This is because a vertical disc is subjected primarily to frictional drag acting on its two sides as opposed to the form drag that acts on a horizontal disc. The reduced drag in turn allows for a greater terminal rise velocity to be reached before the balance

between the buoyant and drag forces acting on the disc is reached. The drag for a vertical disc was calculated assuming a laminar boundary layer was formed on both sides of an infinitely thin disc, and was found to range from 4 to 35 times less than the drag on a corresponding horizontal disc for the range of Reynolds numbers observed. This provided the following equation for the frictional drag force acting on the vertical disc:

$$F_D = 3.28\rho_w \sqrt{\nu}\left(\frac{d}{2}V\right)^{3/2} \qquad [19]$$

where F_D is the total frictional drag force acting on the two sides of a disc of diameter d. The net buoyant force F_B acting on the particle is given by:

$$F_B = (\rho_w - \rho_i) g \pi \frac{d^2}{4} t \qquad [20]$$

The drag force and buoyant force are in balance (i.e. $F_B = F_D$) when a particle is rising at its terminal rise velocity and equating equations [19] and [20] and rearranging gives the following equation for the rise velocity of a vertical disc:

$$V = \left[\frac{\pi(\rho_w - \rho_i) g t}{3.28\rho_w}\sqrt{\frac{d}{2\nu}}\right]^{2/3} = \left[\frac{\pi g' t}{3.28}\sqrt{\frac{d}{2\nu}}\right]^{2/3} \qquad [21]$$

Equation [21] was then solved for a number of different aspect ratios and it was found that the faster moving particles could be represented reasonably well by the

curve corresponding to an aspect ratio of 10 (Figure 3-11). As can be seen by the linear plot in Figure 3-11, an equation in which V is directly proportional to d is obtained when a constant d/t ratio is substituted into equation [21]. This scenario offers a much more realistic alternative to that of a horizontal disc with an aspect ratio of two. The data points in Figure 3-11 are also categorised based on particle Reynolds number and when comparing to the curve corresponding to equation [21] with an aspect ratio of 10, it is seen that many of the faster particles have values of *Re* between 1 and 5. However, this does not necessarily mean that the discs would have stabilised to the horizontal as was suggested by Willmarth et al. (1964), as they noted that this only occurred for Reynolds numbers *approximately* between 1 and 100, and Zhong and Lee (2012) only confirmed this for Reynolds numbers as small as 40. The enveloping aspect ratios of 10 and 80 are also quite close to the 11 to 71 range observed in the particles with measurable thicknesses, which reinforces the conclusion that these aspect ratios are reasonable upper and lower limits.

Another possibility that was explored was that of a disc having a constant thickness and therefore a changing aspect ratio, rather than vice versa as has been previously assumed. It was suggested by Wuebben (1984) that the solution for a horizontal disc with a constant thickness of 0.05 mm offered a reasonable fit to his data for particle diameters ranging from 1 to 4 millimetres. This, he noted, supports the theory that particles will grow preferentially in the direction normal to the *c*-axis (i.e. with increasing diameter). In Figure 3-11 curves for constant

particle thicknesses of 0.05 mm and 0.07 mm are plotted and it can be seen that the curves pass through the cluster of data in the 0.5 to 1.0 mm diameter range that also corresponds well to the curve for a horizontal disc with an aspect ratio of 10 (Figure 3-10). However, it is difficult to say if one thickness is more correct than the other, as it was only possible to measure the thicknesses of 38 particles in this study, and significantly more data would be required in order to definitively determine the average thickness of frazil particles.

While the primary reason for varying the propeller speed and air temperature between experiments was for determining the impact of these variables on the particle size distribution, the possibility that these variables affected the rise velocity was also explored. The only noticeable difference found was that no particles larger than 1.76 mm in diameter were observed in the two 325 rpm experiments. However, considering the same window of time since the propellers had been switched off, the rise velocities measured during the 325 rpm experiments were found to be statistically similar at the 5% significance level to those measured in the 125 rpm experiments.

3.7 Conclusions

The rise velocity of frazil ice particles was investigated by analysing data obtained in five laboratory experiments. Particles were observed with rise velocities ranging from 0.40 to 13.47 mm/s and diameters ranging from 0.24 to 3.35 mm. Theoretical solutions for the rise velocity of horizontal discs with varying diameter to thickness ratios were compared to the data, and it was found

that the data could be enveloped by curves corresponding to ratios of 2 and 80 for a horizontal disc using the solution derived by Gosink and Osterkamp (1983). A theoretical solution was derived for the case of a vertical disc experiencing frictional drag and this expression solved for an aspect ratio of 10 represents a more realistic hypothesis for the faster moving particles. Thicknesses ranging from 0.03 to 0.12 mm with a mean of 0.07 were measured for 38 particles captured in the suspended frazil images, and their aspect ratios were found to range from 11 to 71. This supported the hypothesis that the discs tend to have an increasing aspect ratio due to preferential growth normal to the *c*-axis, and reinforced the conclusion that aspect ratios of 10 and 80 are reasonable envelope values. The cases representing horizontal discs with thicknesses of 0.05 and 0.07 mm were found to fit much of the data well, passing through many of the data points in the 0.25 to 1.75 mm diameter range. The variables of propeller speed in the tank and air temperature in the cold room were not observed to have any effect on the particle rise velocity.

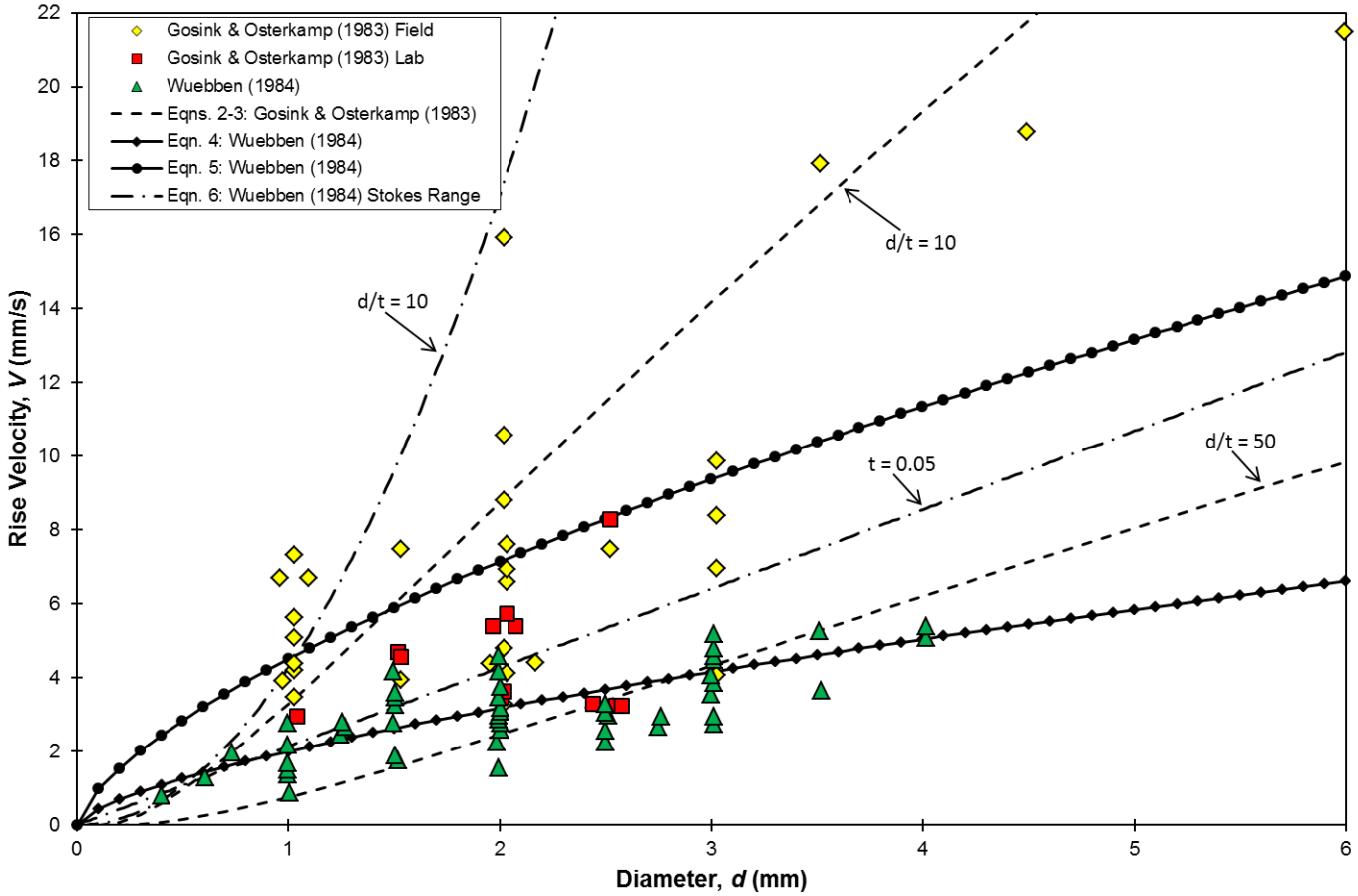

Figure 3-1: Rise velocity of frazil ice particles plotted as a function of particle diameter. Data collected by Gosink and Osterkamp (1983) and Wuebben (1984) is shown, as well as the theoretical solutions presented in those two studies.

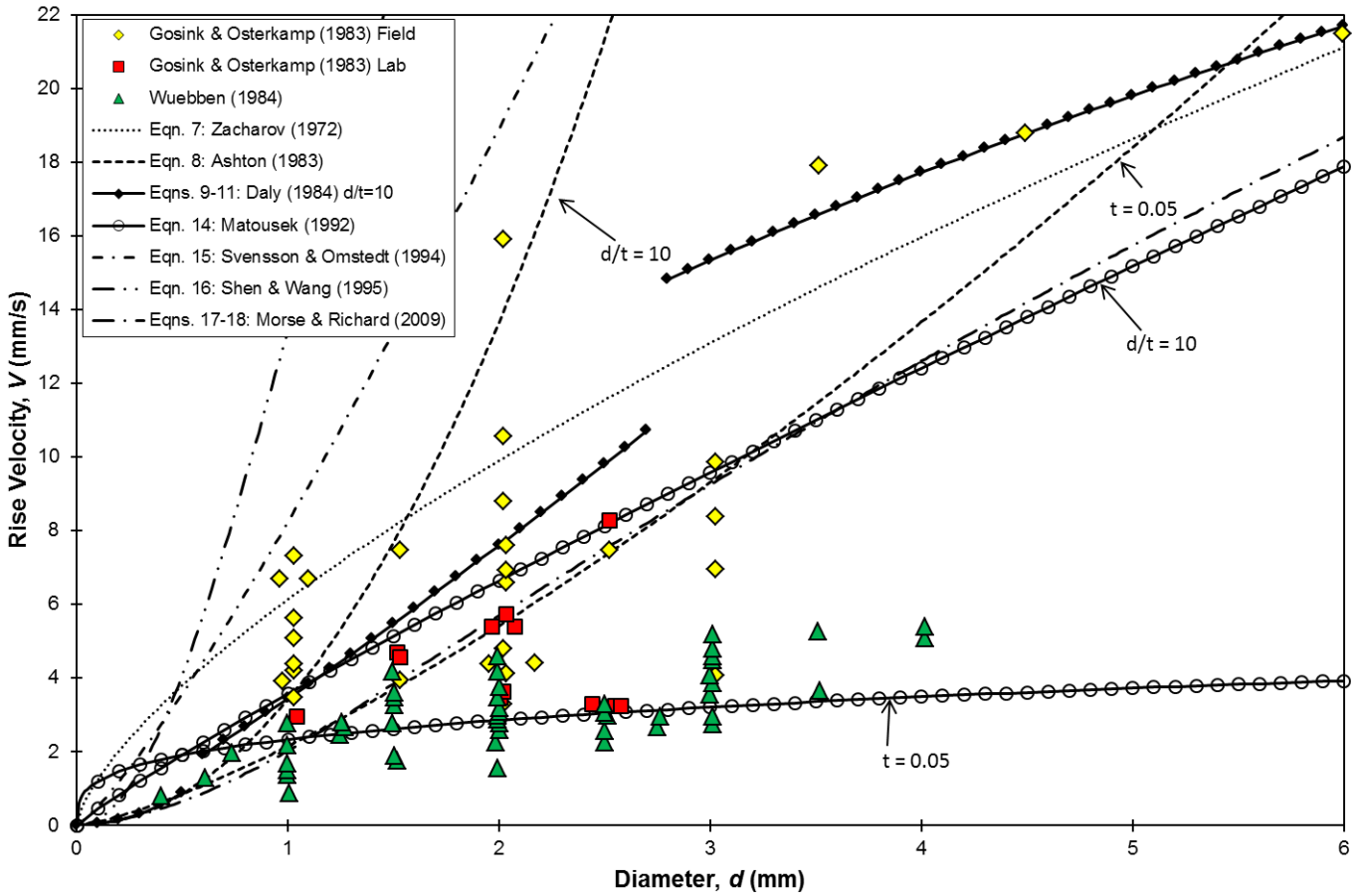

Figure 3-2: Comparison of other existing theoretical models to Gosink and Osterkamp's (1983) and Wuebben's (1984) measured rise velocity data.

a)

b)

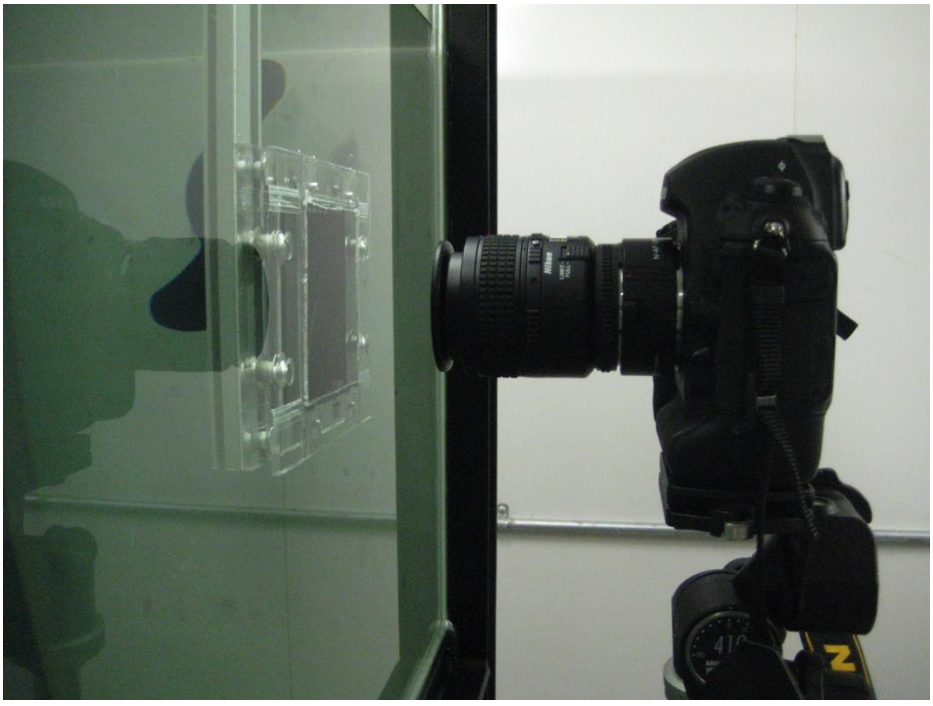

Figure 3-3: a) Rear view of the frazil ice production tank, and b) the camera mounted with the lens 55 mm from the glass. The two polarizing filters are seen inside the tank.

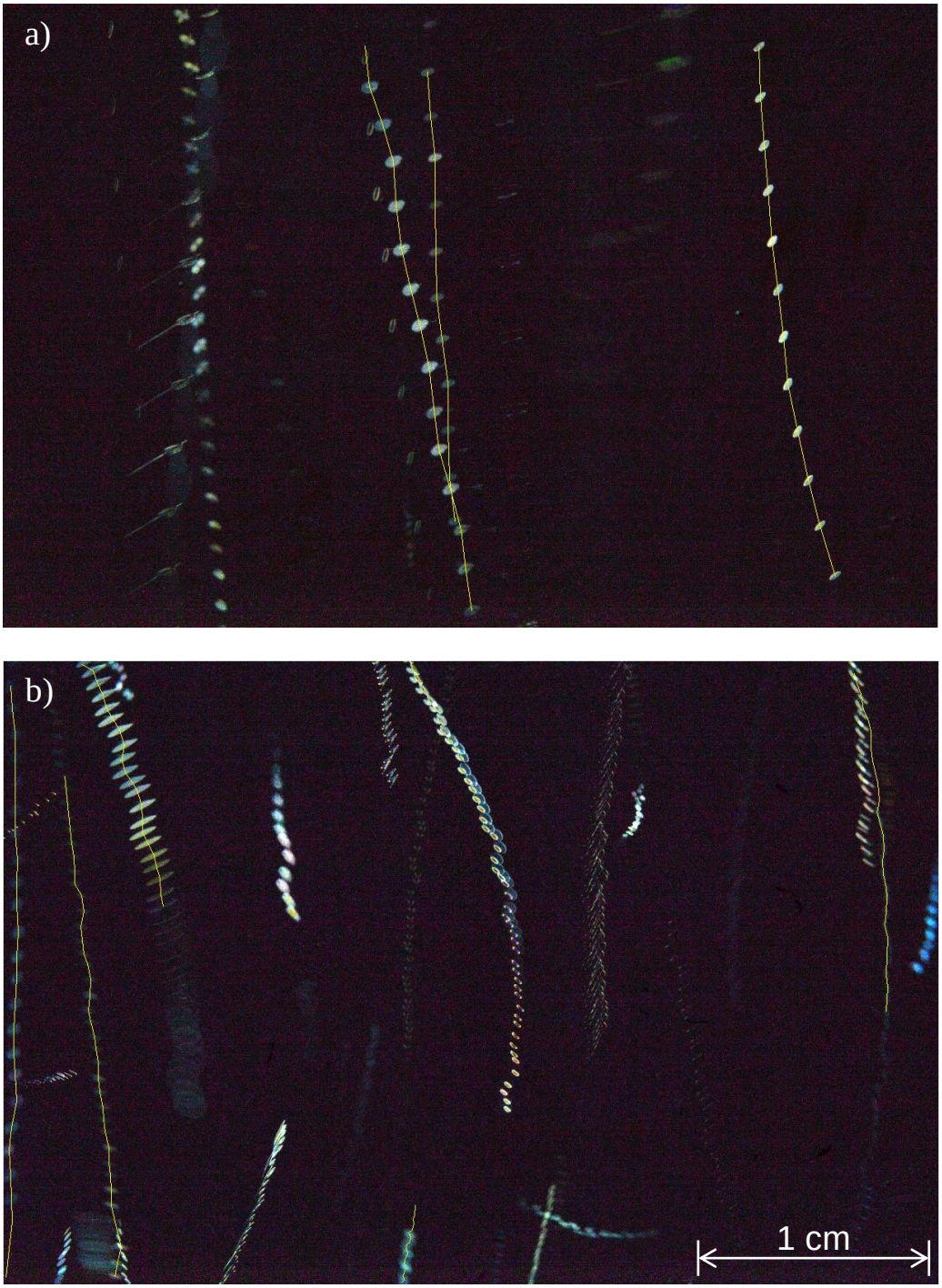

Figure 3-4: Two time-lapse digital images, each consisting of 50 superimposed rise velocity images for a) Experiment 40, approximately 2.5 minutes after the propellers had been switched off, and b) Experiment 49, approximately 5 minutes after the propellers had been switched off. The yellow lines show the path of the centroid of a tracked particle.

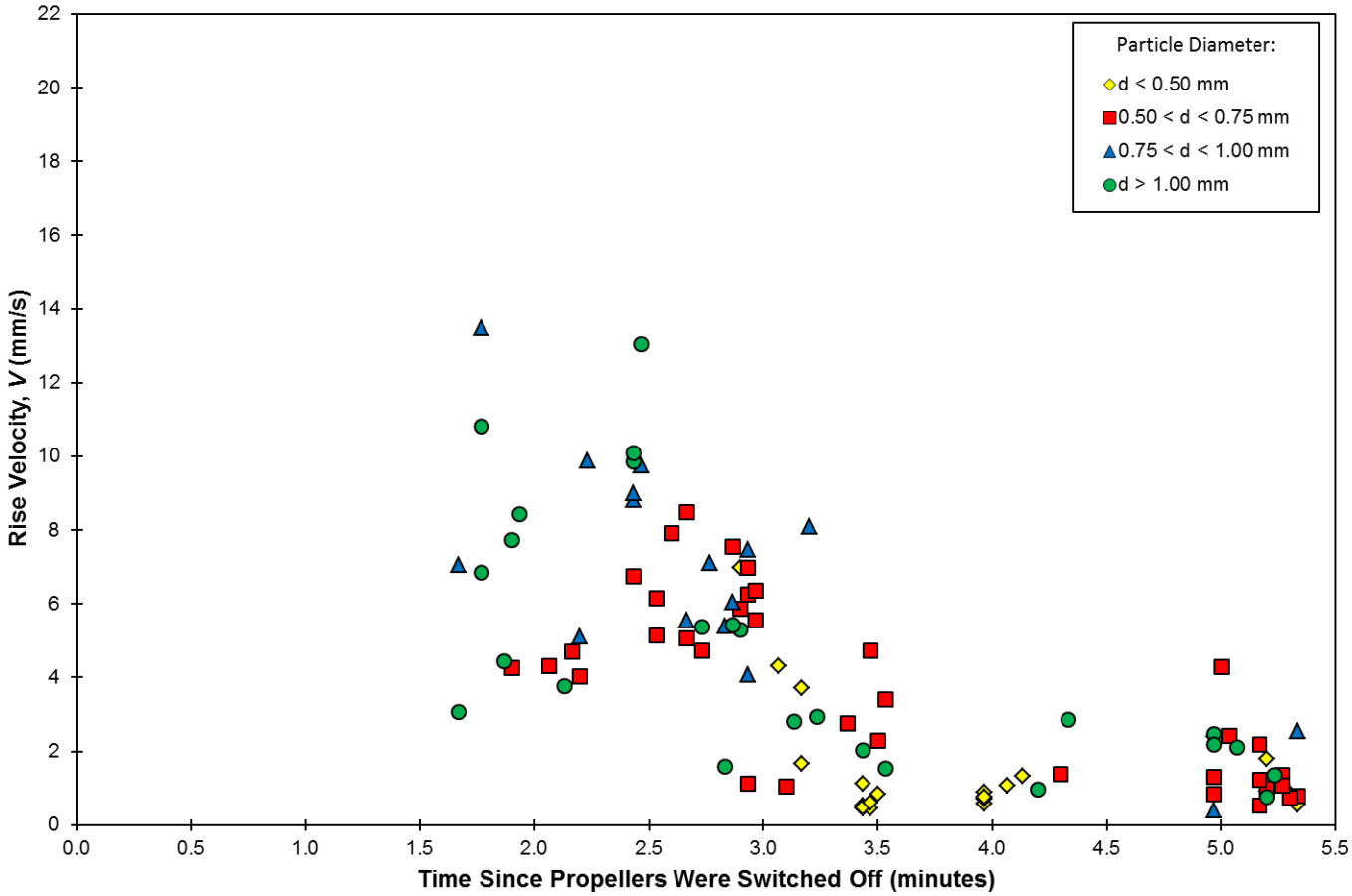

Figure 3-5: Rise velocity plotted as a function of the approximate time since the propellers had been switched off. Data points are distinguished from each other based on the particle diameter.

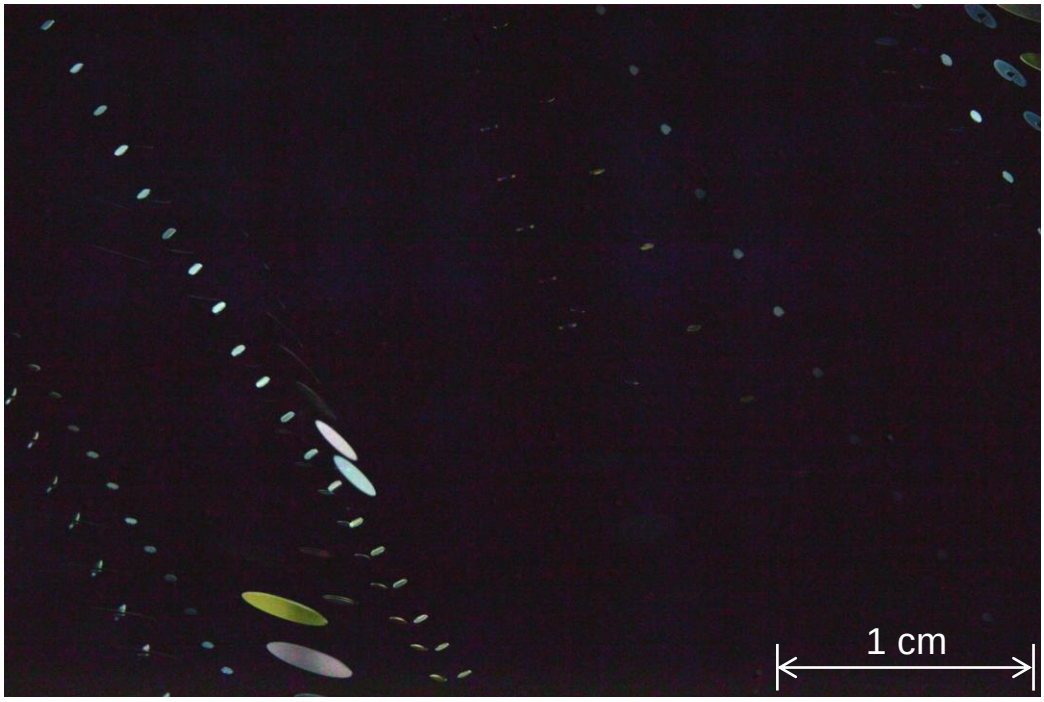

Figure 3-6: A series of 50 superimposed images from Experiment 43. The similar trajectory of all of the visible particles clearly indicates the influence of a residual current in the tank, and thus this data was not included in the final analysis.

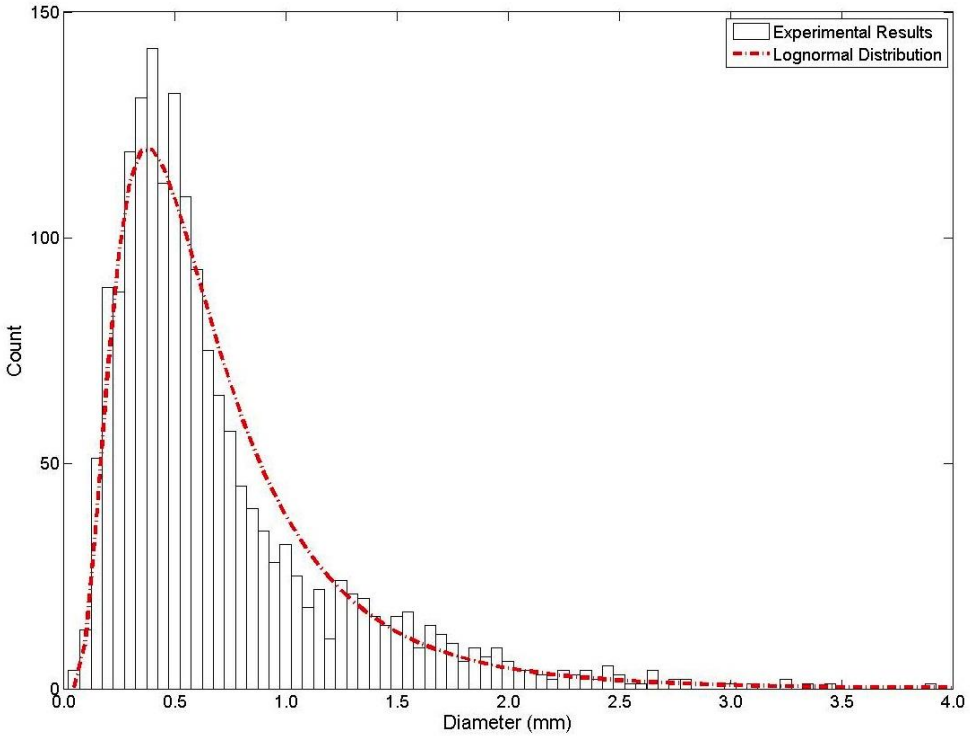

Figure 3-7: A histogram of the size distribution of suspended frazil ice particles observed prior to particle flocculation for experiment 47, fit with a lognormal distribution. The data shown has a mean particle diameter of 0.70 mm and a standard deviation of 0.52 mm for a total of 1797 frazil particles.

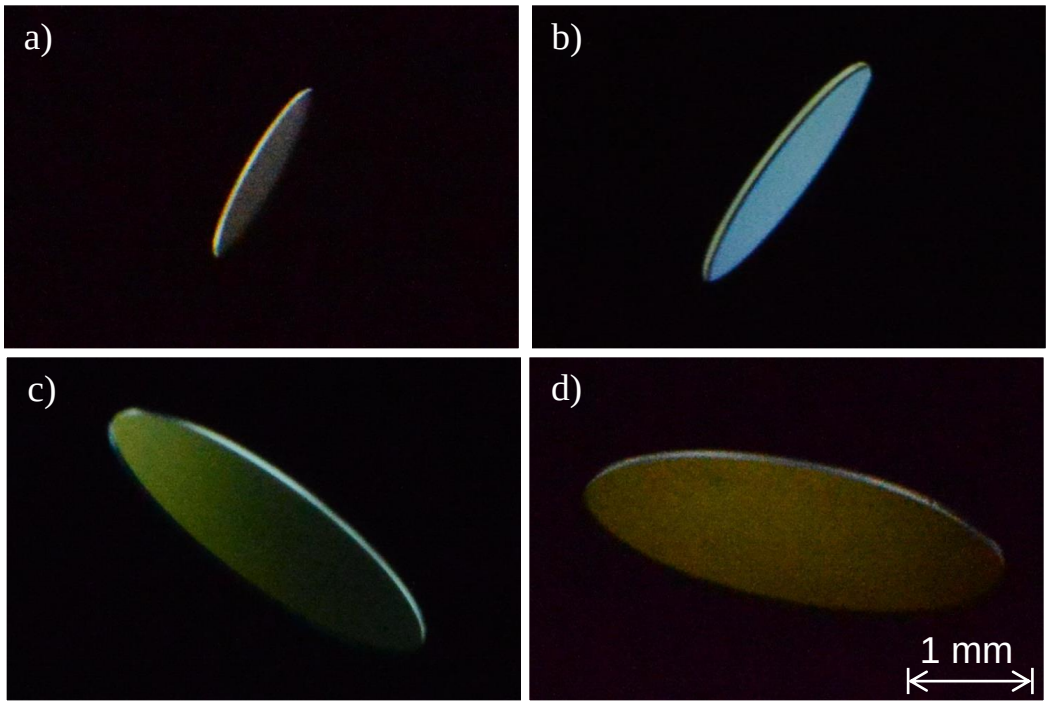

Figure 3-8: Example images in which particle thicknesses were measureable. The particles had the following properties: a) d = 1.53 mm, t = 0.05 mm, and d/t = 30; b) d = 2.17 mm, t = 0.08 mm, and d/t = 27; c) d = 3.08 mm, t = 0.06 mm, and d/t = 49; and d) d = 3.43 mm, t = 0.05 mm, and d/t = 71.

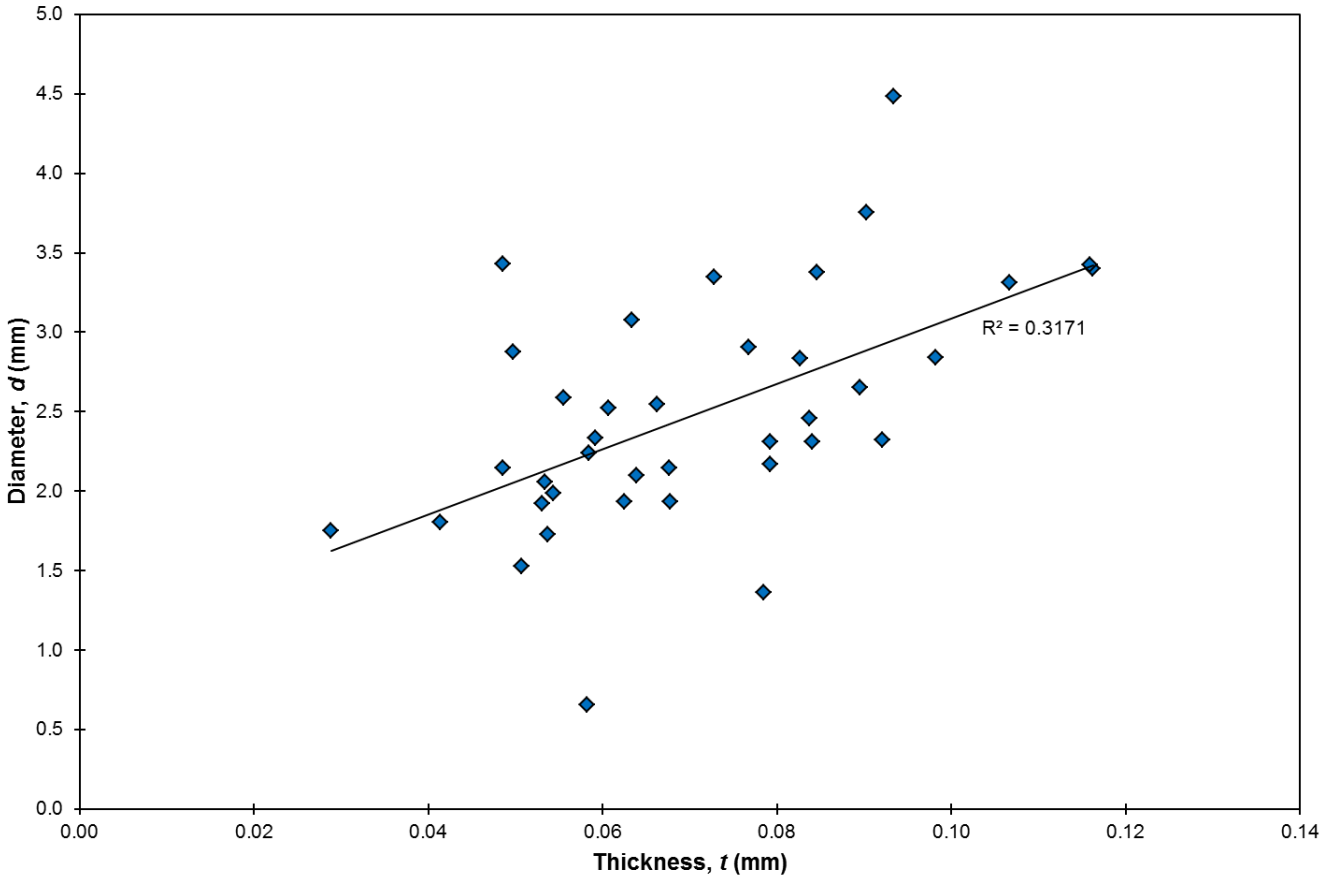

Figure 3-9: Particle diameter plotted versus particle thickness for the 38 suspended frazil particles in which the thickness was measureable. It can be seen by the low R^2 value in the linear regression curve fit to the data that no strong relationship between diameter and thickness exists.

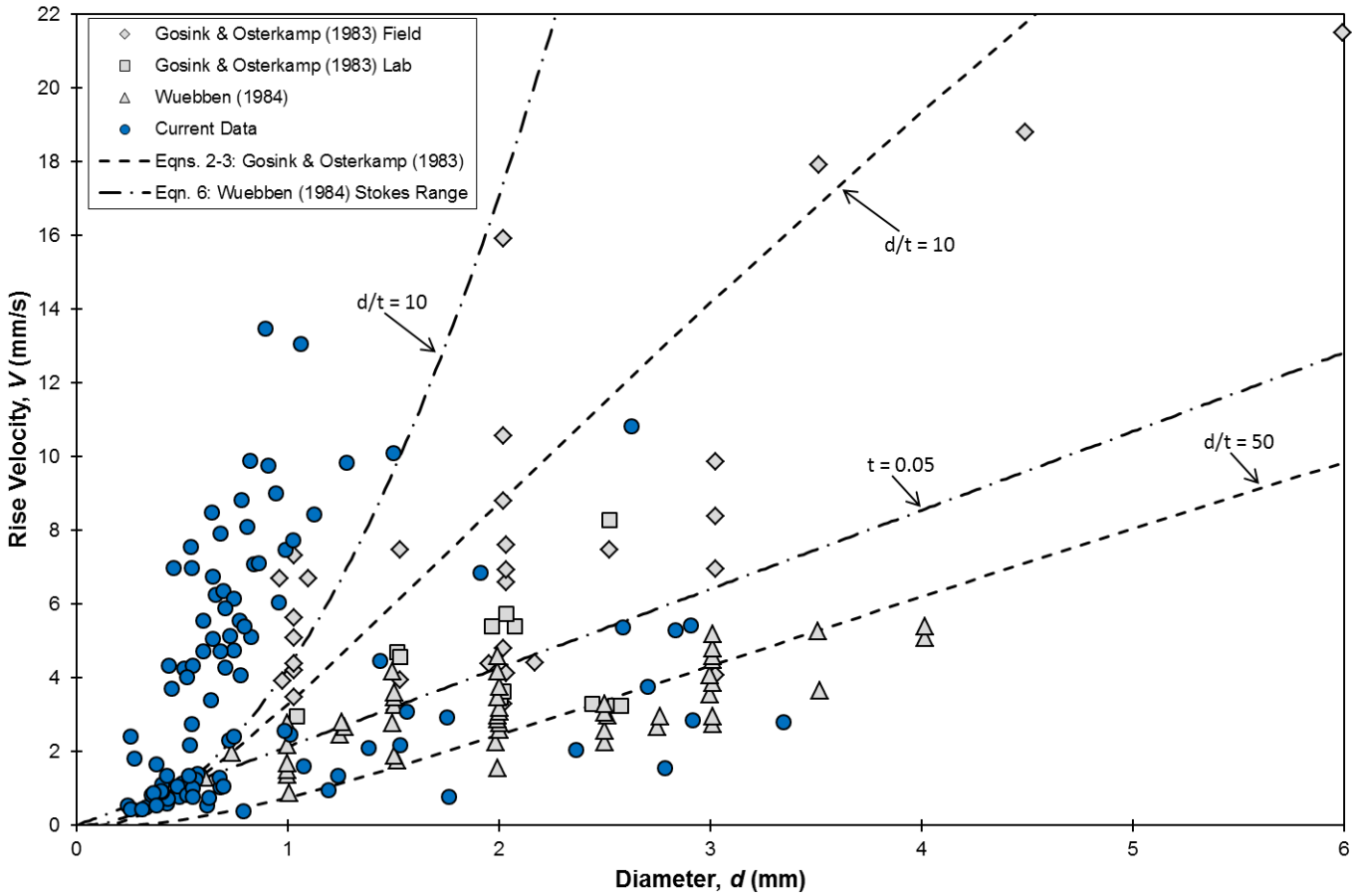

Figure 3-10: Rise velocity of frazil ice particles plotted as a function of particle diameter. The data from the current study is presented along with the data and theoretical curves given by Gosink and Osterkamp (1983) and Wuebben (1984).

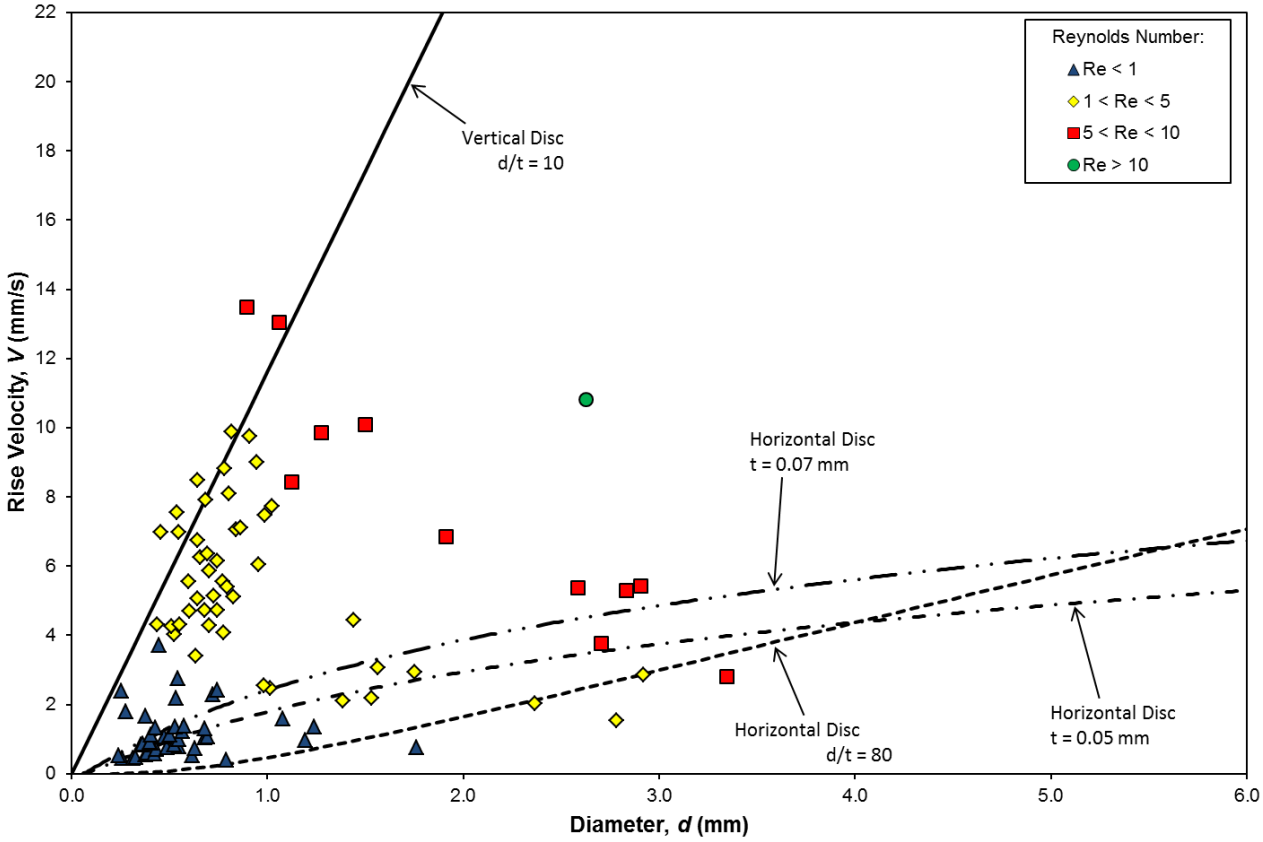

Figure 3-11: Rise velocity of frazil ice particles plotted as a function of particle diameter. Data points have been distinguished from each other based on the particle Reynolds number, and curves corresponding to equation [19] for an aspect ratio of 10 and equations [2] and [3] for an aspect ratio of 80 are shown to envelope the data. Equations [2] and [3] for constant thicknesses of 0.05 and 0.07 mm are also shown.

Table 3-1: Characteristics of each experiment. Propeller speed and air temperature were varied to determine how the size distribution of frazil particles is affected by each of these variables. No noticeable influence of these variables on rise velocity was observed.

Experiment #	Propeller speed (rpm)	Air temperature (^{o}C)
27	325	-10
37	125	-10
38	125	-10
40	125	-10
49	325	-5

References

Ashton, G.D., 1983. Frazil Ice, in: Theory of Dispersed Multiphase Flow. Academic Press, pp. 271–289.

Clark, S., 2013. Border and Skim Ice, in: Beltaos, S. (Ed.), River Ice Formation. Committee on River Ice Processes and the Environment, CGU-HS, Edmonton, Alberta, pp. 77–106.

Clark, S., Doering, J., 2006. Laboratory Experiments on Frazil-Size Characteristics in a Counterrotating Flume. J. Hydraul. Eng. 132, 94–101.

Clark, S., Doering, J.C., 2004. A laboratory study of frazil ice size distributions, in: Proceedings of the 17th International Symposium on Ice. International Association of Hydraulic Engineering and Research, Saint Petersburg, Russia, pp. 291–297.

Daly, S.F., 1984. Frazil Ice Dynamics. Cold Regions Research & Engineering Laboratory, Hanover, N. H.

Daly, S.F., 1994. Report on frazil ice. Cold Regions Research & Engineering Laboratory, Hanover, N. H.

Daly, S.F., Colbeck, S.C., 1986. Frazil ice measurements in CRREL's flume facility, in: Proceedings of the IAHR Ice Symposium 1986. International Association for Hydraulic Research, Iowa City, Iowa, USA, pp. 427–438.

Doering, J.C., Morris, M.P., 2003. A digital image processing system to characterize frazil ice. Can. J. Civ. Eng. 30, 1.

Fujioka, T., 1978. Study of ice growth in slightly undercooled water. Carnegie-Mellon University.

Ghobrial, T., Loewen, M., Hicks, F., 2009. Frazil Ice Measurements Using the Shallow Water Ice Profiling Sonar, in: 15th Workshop on River Ice. CGU HS Committee on River Ice Processes and the Environment, St. John's, Newfoundland and Labrador.

Gosink, J.P., Osterkamp, T.E., 1983. Measurements and Analyses of Velocity Profiles and Frazil Ice-Crystal Rise Velocities during periods of Frazil-Ice Formation in Rivers. Ann. Glaciol. 79–84.

Hammar, L., Shen, H.T., 1991. A Mathematical Model for Frazil Ice Evolution and Transport in Channels, in: Proceedings of the 6th Workshop on the

Hydraulics of Ice Covered Rivers. Committee on River Ice Processes and the Environment, Ottawa, Ontario, Canada, pp. 201–216.

Healy, D., Hicks, F.E., 2007. Experimental Study of Ice Jam Formation Dynamics. J. Cold Reg. Eng. 20, 117–139.

Khvorostyanov, V.I., Curry, J.A., 2002. Terminal Velocities of Droplets and Crystals: Power Laws with Continuous Parameters over the Size Spectrum. J. Atmos. Sci. 59, 1872–1884.

Khvorostyanov, V.I., Curry, J.A., 2005. Fall Velocities of Hydrometeors in the Atmosphere: Refinements to a Continuous Analytical Power Law. J. Atmos. Sci. 62, 4343–4357.

Matoušek, V., 1992. Frazil and skim ice formation in rivers, in: Proceedings of the 11th International Symposium on Ice. International Association for Hydraulic Engineering & Research, Banff, Alberta, pp. 1–22.

McFarlane, V., Loewen, M., Hicks, F., 2012. Laboratory Experiments to Determine Frazil Ice Properties, in: Proceedings of the Annual Conference and General Meeting of the CSCE - 2012. Edmonton, Alberta, pp. 1–10.

Morse, B., Richard, M., 2009. A field study of suspended frazil ice particles. Cold Reg. Sci. Technol. 55, 86–102.

Rubey, W.W., 1933. Settling velocities of gravel, sand, and silt particles. Am. J. Sci. 25, 325–338.

Schlichting, H., 1968. Boundary-Layer Theory, Sixth Edit. ed. McGraw-Hill, New York.

Shen, H.T., Wang, D.S., 1995. Under Cover Transport and Accumulation of Frazil Granules. J. Hydraul. Eng. 121, 184–195.

Shulyakovskii, L.G., 1960. Ice production and freeze-up date in rivers, lakes and reservoirs (Estimates for forecast purposes). Gidrometeoizdat, Moscow.

Svensson, U., Omstedt, A., 1994. Simulation of Supercooling and Size Distribution in Frazil Ice Dynamics. Cold Reg. Sci. Technol. 22, 221–233.

Willmarth, W.W., Hawk, N.E., Harvey, R.L., 1964. Steady and Unsteady Motions and Wakes of Freely Falling Disks. Phys. Fluids 7, 197–208.

Wuebben, J.L., 1984. The Rise Pattern and Velocity of Frazil Ice, in: Proceedings of the 3rd Workshop on the Hydraulics of Ice Covered Rivers. Committee on

River Ice Processes and the Environment, Fredericton, New Brunswick, Canada, pp. 297–316.

Zakharov, V.P., Beilinson, M.M., Shatalina, I.N., 1972. Specific Features of Ice Conditions in Rivers and Reservoirs of Central Asia, in: Proceedings of the IAHR Symposium on Ice and Its Action on Hydraulic Structures. International Association for Hydraulic Engineering & Research, Leningrad, USSR, pp. 224–228.

Zhong, H.-J., Lee, C.-B., 2012. The wake of falling disks at low Reynolds numbers. Acta Mech. Sin. 28, 367–371.

Chapter 4: Summary and Conclusions

Currently there is no practical means of measuring suspended frazil ice concentrations in the field. Although upward looking sonar instruments have been shown to detect frazil ice particles in river flows at various concentrations (Ghobrial et al. 2013a; b; Marko and Jasek 2010a; b), the accuracy of the estimated concentrations and particle sizes has not been verified. Daly and Colbeck (1986) were able to measure particles ranging in diameter from 35 μm to ~0.5 mm, and Clark and Doering (2006) could measure particles with diameters 165 μm and above, but neither study was able to observe this entire range of particle sizes at the same time. In both studies it was concluded that a lognormal distribution was a good fit to the observed data.

The size distribution, thickness, and rise velocity of frazil ice particles has been difficult to measure accurately in the past. As a result, our understanding of how these properties influence freeze-up processes and ice cover formation is quite limited. The rise velocity of frazil ice particles in quiescent water, for example, is an important variable in determining whether skim ice will form at freeze-up, or if ice particles at the water surface will become entrained in the flow leading to the production of frazil flocs, pans, and rafts (Matoušek 1992). The diameter, thickness, and aspect ratio of frazil ice particles is also important for modeling the rise velocity in order to determine whether models that assume a constant aspect

ratio (e.g. Gosink and Osterkamp 1983) or constant thicknesses (Wuebben 1984) are more accurate.

In order to address these needs controlled laboratory experiments were conducted in a frazil ice tank. The propeller speed and air temperature, which influence the variables of turbulence intensity and cooling rate, respectively, were varied, though neither of these variables were observed to have any significant impact on the particle rise velocities. An image acquisition and processing system similar to the one used by Doering and Morris (2003) and Clark and Doering (2006, 2008) was developed to capture high-resolution, cross-polarised photographs of the suspended frazil ice particles. Digital image processing algorithms were developed and used to estimate diameters, thicknesses and rise velocities of the frazil ice particles captured in these high-resolutions images.

4.1 Size Distribution

The image acquisition system was refined during a series of preliminary experiments using a 12.1 megapixel Nikon D3 DSLR camera, and the image-processing algorithm was shown to correctly identify individual frazil ice particles even when frazil ice flocs were present in the images. In these preliminary experiments 2954 particles were measured prior to flocculation and 15757 were observed after flocculation had commenced. In the pre-flocculation data set the particles had a mean diameter of 0.80 mm with a standard deviation of 0.56 mm. The post-flocculation data had a mean diameter of 0.72 mm with a standard deviation of 0.47 mm. These two data sets were compared to each other using

Levine's test for equality of variances and it was found that they were not statistically similar, indicating that the size distribution of frazil ice seems to vary with time. However, a lognormal distribution was found to offer a suitable fit to the data in both cases. Additionally, the resolution of these images was high enough that particles as small as 38.9 μm and as large as 5 mm in diameter were observed, effectively spanning the entire range observed by Daly and Colbeck (1986) and Clark and Doering (2006).

4.2 Rise Velocity, Thickness, and Aspect Ratio

The resolution of the image acquisition system was significantly increased by the use of a 36 megapixel Nikon D800 DSLR camera. In addition to capturing suspended frazil particles for the purpose of studying the size distribution, particles were also photographed at a rate of 4 frames per second as they ascended between the polarising filters once the turbulence in the tank had dissipated. Using the image-processing algorithm, the diameter was calculated for each of the rising particles, and the vertical movement of its centroid was tracked to determine the rise velocity. Rising particles with diameters ranging from 0.24 to 3.35 mm were observed with vertical velocities from 0.40 to 13.47 mm/s. Thicknesses were also measured for 38 individual frazil particles and found to range from 0.03 to 0.12 mm with a mean of 0.07 mm, and aspect ratios ranged from 11 to 71. This supports the hypothesis that frazil ice particles grow preferentially in the direction normal to the *c*-axis, as suggested by other researchers (e.g. Clark and Doering, 2006; Daly and Colbeck, 1986; Daly, 1994; Wuebben, 1984), and therefore that assuming that the aspect ratio increases as

particles grow is more realistic than assuming it remains constant when predicting frazil ice rise velocities.

It was observed that many of the discs were rising with orientations that were not perfectly horizontal. To account for this, a simple force balance equation was derived for a disc with a vertical orientation by considering the effects of frictional drag on the two broad crystal faces, as opposed to the effects of form drag that dominate for a horizontal disc. The measured rise velocity data was found to be enveloped by curves corresponding to a vertical disc with an aspect ratio of 10 and a horizontal disc with an aspect ratio of 80, representing the upper and lower bounds, respectively, and the two extreme particle orientations. The fact that the range of observed aspect ratios from 11 to 71 is very close to the aspect ratios of 10 and 80 suggests that these upper and lower bounds on the rise velocity are reasonable. In addition, this indicates that the orientation of a frazil disc is a more important factor than has been assumed in previous studies of rise velocity. The Reynolds numbers observed for the rising particles also indicated that the discs would not necessarily stabilise in the horizontal position but may in fact maintain whatever orientation they had when they began their ascent. It had been previously suggested by Willmarth et al. (1964) that discs with particle Reynolds numbers between approximately 1 and 100 would stabilise horizontally. However, of the 99 tracked particles, 41 of them had values of *Re* less than one, and all but one particle had a Reynolds number less than 10. It was also observed that curves corresponding to a horizontal disc with a constant thickness of 0.05

and 0.07 mm passed through a large portion of the data in the 0.25 to 1.75 mm diameter range.

4.3 Summary and Recommendations for Future Studies

The size distribution and rise velocity of frazil ice particles are two important factors in the river freeze-up process, and in order to understand one we must understand the other. An imaging system was developed to accurately measure the diameters, thicknesses, and rise velocities of individual frazil ice particles. This data was used to investigate the effects of particle diameter, thickness, and aspect ratio on the kinematics of frazil rise in quiescent water. For the first time, particles were observed to rise with orientations other than perfectly horizontal, indicating that it is important to consider all possible particle orientations in between the extreme horizontal and vertical cases when calculating possible rise velocities.

The impact of different variables, such as propeller speed (and therefore turbulence intensity) and air temperature (which influences cooling rate) on the particle size distribution was not investigated, as these variables were held constant for the experiments described in Chapter 2. However, turbulence intensity has been shown to impact the mean frazil particle size in the past (Clark and Doering 2008), and the effects of this along with the cooling rate will be explored in future work. Different mean particle sizes were observed in the pre- and post-flocculation stages in these experiments, indicating that the particle size distribution changes with time, and this will also be explored in detail in future

studies. The possibility exists for adapting this particle imaging system for use in the field as well, allowing for direct measurements of size distributions in rivers.

In future rise velocity experiments images could be captured sooner after the propellers had been switched off in order to capture the fastest moving particles before they have passed through the sample volume. To make this possible a system could be developed to damp out or dissipate the residual currents quicker to ensure that there is no influence of these currents on the particle velocities. The propellers could also be switched off earlier in the experiments once the suspended frazil ice concentration has peaked but before flocculation has commenced and this would allow more particles to be imaged and analysed. This data will be important for understanding the impact of different river characteristics on frazil ice properties, which is necessary information for quantifying the suspended frazil ice concentrations measured by sonar instruments in different streams, and for the development of future mathematical models of the formation, evolution, and transport of frazil ice.

References

Clark, S., and Doering, J. (2006). "Laboratory Experiments on Frazil-Size Characteristics in a Counterrotating Flume." *Journal of Hydraulic Engineering*, American Society of Civil Engineers, 132(1), 94–101.

Clark, S., and Doering, J. (2008). "Experimental investigation of the effects of turbulence intensity on frazil ice characteristics." *Canadian Journal of Civil Engineering*, 35(1), 67–79.

Daly, S. F. (1994). *Report on frazil ice*. Cold Regions Research & Engineering Laboratory, Hanover, N. H., 50 pages.

Daly, S. F., and Colbeck, S. C. (1986). "Frazil ice measurements in CRREL's flume facility." *Proceedings of the IAHR Ice Symposium 1986*, International Association for Hydraulic Research, Iowa City, Iowa, USA, 427–438.

Doering, J. C., and Morris, M. P. (2003). "A digital image processing system to characterize frazil ice." *Canadian Journal of Civil Engineering*, Canadian Science Publishing, 30(1), 1.

Ghobrial, T. R., Loewen, M. R., and Hicks, F. E. (2013a). "Continuous monitoring of river surface ice during freeze-up using upward looking sonar." *Cold Regions Science and Technology*, Elsevier B.V., 86, 69–85.

Ghobrial, T. R., Loewen, M. R., and Hicks, F. E. (2013b). "Characterizing suspended frazil ice in rivers using upward looking sonars." *Cold Regions Science and Technology*, Elsevier B.V., 86, 113–126.

Gosink, J. P., and Osterkamp, T. E. (1983). "Measurements and Analyses of Velocity Profiles and Frazil Ice-Crystal Rise Velocities during periods of Frazil-Ice Formation in Rivers." *Annals of Glaciology*, 79–84.

Marko, J. R., and Jasek, M. (2010a). "Sonar detection and measurements of ice in a freezing river I: Methods and data characteristics." *Cold Regions Science and Technology*.

Marko, J. R., and Jasek, M. (2010b). "Sonar detection and measurement of ice in a freezing river II: Observations and results on frazil ice." *Cold Regions Science and Technology*.

Matoušek, V. (1992). "Frazil and skim ice formation in rivers." *Proceedings of the 11th International Symposium on Ice*, International Association for Hydraulic Engineering & Research, Banff, Alberta, 1–22.

Willmarth, W. W., Hawk, N. E., and Harvey, R. L. (1964). “Steady and Unsteady Motions and Wakes of Freely Falling Disks.” *The Physics of Fluids*, 7(2), 197–208.

Wuebben, J. L. (1984). “The Rise Pattern and Velocity of Frazil Ice.” *Proceedings of the 3rd Workshop on the Hydraulics of Ice Covered Rivers*, Committee on River Ice Processes and the Environment, Fredericton, New Brunswick, Canada, 297–316.